Forecasting Research

Forecasting Research Division
Scientific Paper No. 44

PERFORMANCE OF THE UNIFIED MODEL

by

S F Milton and C A Wilson

December 1996

Meteorological Office
London Road
Bracknell
Berkshire
RG12 2SZ
United Kingdom

Forecasting Research Division
Scientific Paper No. 44

PERFORMANCE OF THE UNIFIED MODEL

by

S F Milton and C A Wilson

December 1996

PERFORMANCE OF THE UNIFIED MODEL

(Presented at the 1st Met.Office Scientific Advisory Committee (MOSAC), 11/12 November 1996)

S.F. Milton and C.A Wilson, NWP Division.

1. INTRODUCTION

This paper outlines the recent performance of the UK Meteorological Office (UKMO) Unified Model (UM) used for NWP (Cullen, 1993). Three model configurations are currently used for operational forecasting; the Global, Limited Area (LAM) and Mesoscale models. For brevity we concentrate most of our attention on the Global NWP model but do discuss some recent developments in LAM and Mesoscale configurations. Section 2 outlines the formulation of the models. Section three discusses the main aspects of the performance of the Global model, concentrating on known systematic errors and the improvements made to the models since its introduction in 1991. Recent improvements to LAM and Mesoscale data assimilation is discussed in section four. In section five we discuss the performance of the UM in terms of standard verification measures. Finally, we highlight forthcoming improvements to the UM in section six and give a summary in section seven.

2. MODEL CONFIGURATIONS

2.1 Model resolutions, numerics and data assimilation

The vertical and horizontal resolutions and time step of the UM configurations are shown below.

	LAT	LON	SPECTRAL EQUIV.	RES(km)	T/S	LEVS	RANGE
Global - CLIM	2.5°	3.75°	T42	250	30	19	
Global - NWP	0.83°	1.25°	T106	90	20	19	T+144
LAM	0.442°	0.442°	_	50	5	19	T+48
Mesoscale	0.15°	0.15°	_	17	1.5	31	T+30

The global and LAM versions were introduced in 1991, and the Mesoscale Model was Unified in 1992. This essentially involved a change from non-hydrostatic to hydrostatic dynamics. All models use the split explicit finite difference numerical integrations scheme on the Arakawa B grid. This has an advection timestep of 10 minutes for the global NWP model and three adjustment steps for every advection step. The physics is currently applied every second advection timestep (i.e every 20 minutes). The finite difference equations are second order accurate in space in the global NWP model and fourth order accurate in the global CLIM version. The primitive equations conserve mass, energy, momentum, angular momentum and total water and include a full treatment of the Coriolis terms. Fourier filtering of unstable waves is applied at high latitudes in the global model. A $\nabla 4$ diffusion of

mass-weighted winds, liquid potential temperature and moisture is used. A hybrid coordinate is used in the vertical, with the top three model levels being pure pressure layers.

Observations are assimilated using the the assimilation correction (AC) scheme. This a nudging scheme in which the model state is continuously adjusted back towards the observed state over the assimilation period (6hrs for global:3hours for mesoscale) by the repeated insertion of observations. Variational analysis schemes are currently under development for the UM. The mesoscale data assimilation has undergone several developments in recent years and now includes a cloud analysis (MOPS[1]), and latent heat nudging of the thermodynamic fields. Soil moisture fields were allowed to run free in the model for a period between April 1995 and May 1996 but are now reset weekly to the MORECS[2] values (see section 4).

2.2 Model Physics

Global Model and LAM

a) Convection - A mass flux penetrative convection scheme incorporating downdraughts.

b) Large Scale Cloud and Precipitation - Cloud ice and cloud water are held as model variables; the total water content is the variable advected by the dynamics. Evaporation of precipitation, enhanced precipitation from seeding layers, and phase changes between cloud water and ice are represented.

c) Radiation - six spectral bands are used in the LW and four in the SW. The radiation scheme includes the effect of water vapour, ozone, CO2, and large scale and convective cloud distributions. Cloud radiative properties are functions of cloud water and cloud ice contents.

d) BL Turbulent Mixing - The boundary layer can occupy the lowest five model layers, and is parametrized using a first order turbulent mixing-scheme based on an eddy diffusivity approach. The scheme includes stability dependent transfer coefficients modified by the presence of cloud. Non-local mixing is also carried out for temperature and moisture in unstable conditions. A parametrization of form drag due to subgridscale orography has been recently introduced using an effective roughness length based on orographic and vegetative roughness.

e) Land Surface Processes - A 4 layer soil temperature model is used, and different soil types are specified and used to determine surface albedo. Surface hydrology takes account of storage of water in a vegetative canopy as well as in ground storage. The soil moisture fields in the global model are currently reset daily to climatological values

---

[1]MOPS - Moisture Observation Pre-processing System

[2] Meteorological Office Rainfall and Evaporation Calculation system

f) The gravity wave drag (GWD) scheme is based upon linear theory of hydrostatic gravity waves but since January 1995 also incorporates anisotropy in the orographic variance field and includes the effect of high drag states and trapped lee waves.

g) Vertical Diffusion is applied in the Global NWP model between 30N-30S and model levels eight to 14 (500hPa - 150hPa)

Mesoscale Model

The Mesoscale Model shares most of the physics of the Global model. It contains no GWD scheme but does contain the parametrisation of orographic roughness. No vertical diffusion is applied.

3. GLOBAL MODEL SYSTEMATIC ERRORS

In this section we concentrate on the performance of the global UM for December, January and February (DJF) 1995/96 and June, July and August (JJA) 1995. We highlight known systematic errors in the model and possible causes for these errors. To place the current model performance in context, the impact of the major improvements since 1991 are also briefly discussed. The climate version of the UM is not discussed. However, many of the systematic errors in the NWP version are also apparent in climate simulations (see Kershaw and Slingo(1996) for examples of the cold bias in the two versions)

3.1 Mass and wind fields

Zonally Averaged U and V Winds

In DJF the extratropical zonal wind errors at T+72 (Fig. 1(b)) are symmetric about the equator with westerly errors at 40N-60N and 40S-60S, and easterly errors poleward of these latitudes. The errors in the southern hemisphere (SH) are larger than those in the northern hemisphere (NH). The latter have been reduced since the introduction of the new GWD scheme and orographic roughness in January 1995 (Milton and Wilson, 1996). In the stratosphere at 30N the UM has an easterly bias of -1.5 m/s. This is thought to be associated with excessive gravity wave drag (GWD) still being applied in the stratosphere. This decelleration of the westerlies extends down into the NH jet core. The tropical errors change sign with height; easterly errors occur in the subtropical/tropical boundary layer and westerly errors in the tropical upper troposphere at 20N and 20S. The largest tropical error is an easterly bias of -1.5 m/s at the equator between 200hPa and 100hPa. This error is reduced in the UM when convective momentum transports are introduced (to be implemented in November 1996)

In JJA (Fig. 1(d)) we note similar mean errors in the extratropics. Again the largest errors are in the SH. The tropical errors in the boundary layer show a westerly bias at 10N and easterly bias at

10S associated with an overactive Monsoon circulation. At upper levels we see the same signature as in DJF of an easterly error flanked by westerly errors. The stratospheric easterly bias at 30N in DJF is not present in JJA. This is consistent with the error being linked to excessive GWD.

The T+72 meridional wind errors (Fig 2(c) and 2(d)) show an increase in the Hadley circulation in both seasons, which is confined to the upper levels of the tropical troposphere, and is largest in JJA. Again the introduction of convective momentum transports into the UM reduces this error

Mean Sea Level Pressure (MSLP)

We can see the familar climatological features of the Aleutian and Icelandic lows, subtropical highs and Siberian Anticyclone in the NH DJF analysis (Fig. 3(a)). The SH is dominated by a strong westerly flow at 50S between the subtropical highs and circumpolar trough. The T+72 mean error (Fig. 3(b)) has a characteristic error pattern in both the Pacific and Atlantic in the NH, with high pressure to the southwest and low pressure to the north east. This error gives increased westerly flow at 40N-60N over the eastern ocean basins and leads to an eastward shift of both the Aleutian and Icelandic lows. Other prominent errors in the NH include increased pressure over the north pole, a reduction in the intensity of the Siberian Anticyclone by up to 4hPa, and low pressures over the Rockies. In the SH there is an increase in the strength of the subtropical highs and a deepening of the circumpolar trough. As in the NH this leads to increased westerly flow in mid-latitudes, particularly large donwstream of the Andes Cordillera\Antarctic Peninsula and south of Australia at 60S. The tropics are dominated by a negative error in MSLP which is particularly large over the Andes and the Indian Ocean. The T+72 mean errors in JJA (Fig. 4(b)) are similar to those seen in DJF . Subtropical highs are too intense in both hemispheres, and the SH circumpolar trough is still too deep. The Monsoon trough north of India is too deep in the forecasts by ~6hPa. In general pressures are too low over the major desert regions of the Gobi, the Mojave and the Sahara.

Time evolution of the MSLP bias 1991-1996

The biggest improvement in MSLP mean errors (Fig. 5) came with the introduction of the new GWD scheme and orographic roughness in January 1995. These changes have virtually eradicated the large negative bias that occurred during DJF before the change. The accompanying high pressure error in the subtropics has also been reduced. The impact on the SH errors is less marked, but since January 1995 the high pressure error at 30S-50S has also been reduced.

500hPa Geopotential Height

The 500hPa geopotential height has similar error patterns to the MSLP field. In DJF (Fig. 6(b)) the NH error pattern shows a reduction in the amplitude of the planetary waves. The ridges over the eastern ocean basins are too weak and the climatological troughs over the eastern seaboards are not deep enough. In the SH the circumpolar trough is too deep by up to 40m between 150W and 40E.

Upper Tropospheric Winds

The largest error in the NH subtropical jets at 250hPa (Fig. 7(b)) is a reduction of 8 m/s in the wind speed in the East Asian jet over Japan(140E). We also see an increase in the westerly flow to the south of the jet. This pattern of errors leads to a reduction in the intensity and equatorward shift of the forecast jet. A similar reduction can be seen in the strength of the US-Atlantic subtropical jet. These reduced wind speeds imply a reduction in the vertical shear and may have implications for the life-cycle of baroclinic waves in the UM (see section 3.5). In contrast the eastern sectors of the Pacific and Atlantic ocean basins have increased westerlies, due to an eastward extension of both the Atlantic and Pacific jets.

Stratospheric Winds

It was noted earlier that the zonally averaged easterly bias at 30N extended from the stratosphere into the jet core. A potential candidate for this negative bias is excessive GWD in the stratosphere. The typical error in the zonal wind at 70hPa (Fig.8(b)) shows a good correspondence with the error at 250hPa (Fig. 7(b)), with easterly biases downstream of the Himalayas, Rockies and Alps. A sensitivity experiment (GWDSEN) was carried out in which the GWD vertical stress distribution was altered. All of the gravity wave stress diagnosed at the surface was deposited in the boundary layer and none was applied in the stratosphere. Figure 8(c) shows the impact of this change on the 70hPa zonal wind. Downstream of the Rockies and Alps and over the Himalayas the zonal wind becomes more westerly reducing the easterly biases present in the operational version (cf Fig. 8(b) and 8(d)). This shows that excessive GWD is largely responsible for the systematic errors in stratospheric winds, although we do not advocate removing the GWD completely! The influence of removing the stratospheric GWD is not evident at 250hPa until 4-5 days into the integration. It is believed that reducing the stratospheric GWD during the assimilation may show a larger impact at 250hPa. Preliminary tests of a new tuning of the GWD scheme are underway.

3.2 Temperature

Zonally averaged temperatures

The T+72 errors in temperature in DJF (Fig (9(c)) and JJA (Fig. 9(d)) are dominated by a cold bias of order -1K, which is largest at the tropopause and in the SH lower troposphere. In the NH extratropics the tropopause cold bias is largest in JJA. In the stratosphere and the tropical mid troposphere there is a warm bias of between 0.2K to 0.4K. A warm bias can also be seen in DJF over the NH polar regions in the lower troposphere. These features are discussed further in section 3.6 in relation to the thermal balance in the UM and in the companion paper by Kershaw and Slingo (1996). In the NH in DJF we see a near surface cooling of order -1K. This is caused by excessively cold nightime temperatures over land in winter.

Geographical distribution of the temperature bias at 850, 500 and 250 hPa

At 850hPa the T+72 cold bias in DJF is located over the oceanic "stormtrack" sectors in the NH (Fig 10(a)). For example off the eastern seaboard of the US the UM cools by -1.5K by day three. Over the continents the model forecasts show a warming of order 1K. The SH cooling at 40S extends over all longitudes. There are interesting error maxima in the SH consisting of positive-negative dipoles off the western continents of Australia, South America, and Africa. These errors may be associated with the incorrect modelling of the extensive stratus/stratocumulus cloud decks in these regions. At 500hPa we see similar cooling of the oceanic stormtracks and warming of the land. This error structure of warm bias poleward of a cold bias reduces the equator to pole temperature gradient and is consistent with the reductions in vertical wind shear in the jet entrance regions (Fig. 7). In the tropics the main feature is a warm bias in the east tropical Pacific. At 250hPa the dominant signal is a cooling in both tropics and extratropics. The errors in JJA (not shown) are similar to those in DJF.

Evolution of the temperature bias 1992-1996

Finally, we consider the evolution of the T+72 temperature bias between October 1992 and July 1996. At 850hPa (Fig 11(a)) the cold biases in the NH and SH extratropics are a maximum in the summer months for each hemisphere. This may be related to excessively bright low cloud over the summer oceans (see section 3.4 on Clouds and Radiative forcing). Since the introduction of the revised moisture assimilation in November 1994 the extratropical cold bias has been reduced. In the tropics the UM suffered from a lower tropospheric warm bias until January 1994 when the introduction of downdraughts in convection (2nd Climate physics (Hadam2a)) removed this.

At 300hPa (Fig. 11(b)) the cold bias dominates the extratropics and shows a distinct seasonal cycle with the largest errors from May to September. There was a general reduction in the cold bias with the introduction of fourth order moisture diffusion in March 1993 suggesting that this bias is sensitive to the amount of upper tropospheric moisture. A further reduction is apparent from May 1996

onwards, which coincides with the introduction of the 1DVAR assimilation of TOVS radiances (so called GLOSS[3] change - see Appendix A).

3.3 Hydrological cycle

Global precipitation and evaporation.

The globally averaged precipitation minus evaporation (P-E) is a useful measure of the model's hydrological balance. The P-E is shown for the global model at various forecast ranges in Figure 12(a). On its introduction in June 1991 the global UM suffered from a clear spin up in P-E, caused by a deficit in global precipitation compared to evaporation during the assimilation. Balance was only achieved by day three of the forecasts. Introducing fourth order moisture diffusion in March 1993 reduced the spin up while the changes to the assimilation of moisture in November 1994 largely removed it.

The time series of globally averaged precipitation (Fig.12(b)) shows the deficit in precipitation during the assimilation in early UM versions. For current model formulation the precipitation during the assimilation is greater than the Jaeger climatology (thought to be an underestimate) and undergoes a small spinup in later forecast ranges with values approaching 3 mm/day by day three. The model formulation changes in March 1993 and November 1994 are clearly seen in tropical precipitation which shows a step increase at these times (Fig. 12(c)). Since November 1994 the "spin -up" in tropical precipitation has been replaced by a "spin-down".

Comparison of UM tropical precipitation with satellite based estimates.

In this section we attempt to validate both forecast and analysed tropical precipiation against satellite and climatological estimates. The satellite estimate of precipitation rate (R) is the GOES precipitation index (GPI; Janowiak, 1992) based on cloud top temperature and calculated from the relation, R=(3mm/hr)*(frac)*(hours), where *frac* is the ratio of pixels with temperatures < 253K to the total number of pixels in a specified area, and *hours* are the numbers of hours in the observation period. The precipitation climatologies of Jaeger(1976) and Legates and Willmott (1990) are also used.

Figure 13 shows the tropical precipitation for December 1994. The UM has a generally good representation of the precipitation in the ITCZ. Comparison of the UM precipitation at T+00-T+24 and T+48-T+72 shows the spin-down in the ITCZ. In the extratropical stormtracks there is a spinup in UM precipitation. Compared to GPI the model has less precipitation in the Central Pacific, South

[3] GLOSS - GLobal Sounding System

America, and Central Africa. The deficiency in precipiation is particularly marked over South America in the UM and is also in poor agreement with Jaeger and Legates and Willmott climatologies. The climate model does not suffere from this problem suggesting it may be an initialisation problem. The model has higher precipitation in the Indian Ocean, the ITCZ off Central America and in the Tropical Atlantic. It is also worth noting the large differences between the three observational estimates; GPI, Jaeger, and Legates and Willmott.

Moist Bias in the UM

The time-latitude plot of T+72-T+00 relative humidity differences at 850hPa shows the UM moist bias with an increase in relative humidity in the extratropics which is largest in the summer season of each hemisphere (Fig. 14). This increase in humidity has been reduced since 1991, with the change to moisture assimilation in November 1994 having the most dramatic effect. The spin-up in relative humidity is highly correlated with the cold bias, but additional diagnostics also show an increase in the specific humidity in the UM. There is also an associated spin up in cloud in the model.

3.4 Clouds and Radiative Forcing.

As with precipitation, clouds are difficult to validate on a global scale. This section contrasts the cloud distributions and top of the atmosphere radiative fluxes against satellite and observational based climatologies.

Validation of cloud amounts - UM vs Warren and ISCCP climatologies.

Figure 14 shows zonally averaged total cloud from the UM at T+00 and T+72 and from the surface based cloud climatology of Warren et al. (1986,1988) and the International Cloud Climatology Project (ISCCP; Rossow and Schiffer, 1991). The Warren climatology is based on synoptic observations taken every three hours over land stations from 1971-81, and over the oceans from ship reports covering 1952-81. We have combined the ocean and land data to give the zonal average total cloud cover. The ISCCP total cloud cover is derived from a global reduced resolution infra-red and visible radiances from operational weather satellites. The UM data is for January 1995 and August 1994 with total cloud cover calculated using maximum random overlap assumptions; The Warren data consists of seasonal averages for DJF and JJA; The ISCCP data is for January and August 1988.

The total cloud amounts given by Warren and ISCCP are in good agreement between 60N and 60S, but do not agree over the polar regions. In both seasons the UM has less cloud than either Warren or ISCCP climatologies in the subtropics. Agreement is better in the extratropics and tropics but the UM still underestimates the total cloud cover. There is a large spinup in cloud in August 1994

in the NH. This spinup has been reduced since the change to moisture assimilation in November 1994 (see Appendix A). The cloud amount at T+72 has not altered much with this model change. The spin up in January 1995 is small.

TOA fluxes - comparisons with ERBE.

The top of the atmosphere (TOA) radiative flux comparison between the UM and Earth's Radiation Budget Experiment (ERBE; Barkstrom, 1994) is summarised in the table below showing the global averages. The UM results are for January 1995 and August 1994 and represent daily averages over the period T-06 to T+18. The ERBE data are for January and August 1988. All fluxes are in Watts/m^2. Although there can be considerable interrannual variability in the ERBE TOA fluxes, in general the model errors are very systematic and larger than the variability. The SW cloud forcing (SWCF) and LW cloud forcing (LWCF) are defined as in Slingo and Slingo (1988)

	January		August	
	UM95	ERBE88	UM94	ERBE88
OLR	246.31	233.28	255.33	240.17
Clear sky OLR	270.22	262.18	278.04	268.40
Net SW	239.32	248.87	235.74	245.17
Albedo(%)	34.02	33.13	32.9	30.46
Clear sky albedo(%)	17.23	18.34	15.96	15.57
SWCF	-62.82	-52.73	-54.01	-46.40
LWCF	23.91	27.25	22.71	27.08
Total CF	-38.91	-25.48	-31.3	-19.32.
Net Radiative flux	-6.99	15.59	-19.59	5.00

We note the following errors in the Unified model TOA radiative fluxes.

- OLR is too large\LWCF is too small in the UM
- Planetary albedo is overestimated\SWCF is too large
- Clear Sky OLR is too large
- Clear sky albedos are too small in January.
- Total cloud forcing is too large

The increase in OLR in the UM may be consistent with the lack of cloud noted in the previous section. However, the clear sky OLR is also too large suggesting the increased OLR is not solely due to lack of cloud.

The LWCF diagnostic is generally dominated by high cloud. During January 1995 the UM underestimates the LWCF in the tropics over the Amazon (consistent with the lack of precipitation (Fig.13)), Central Africa, and large areas of the Pacific and Indian Oceans (Fig. 16). Over some regions of the ITCZ the LWCF is overestimated. These areas coincide with those having excessive tropical precipitation off Central America, the Indian Ocean and the tropical Atlantic (see Fig. 13).

The largest error in SWCF in the UM is an increase in the SH at 40S to 50S (Fig. 17(c)). This error is thought to be associated with low clouds having too high water contents, and is particularly marked for low cloud over the oceans in the summer season of each hemisphere. The location of the SH SWCF error in January 1995 is highly correlated with the lower tropospheric cold bias seen in DJF (Fig. 11(b) and 12(a)). The SWCF also appears to be too high for the deep clouds in the ITCZ, particularly in regions where the precipitation is thought to be excessive (see Fig. 13). The lack of cloud over South America is also apparent in the SWCF.

3.6. Thermal and Momentum Balance in the Global UM.

In recent years we have attempted to systematically apply diagnostic tools which might allow us to identify the source of systematic error growth in the UM. An example are the balance diagnostics developed by Klinker and Sardesmukh (1992). The technique involves calculating the initial thermal, momentum or moisture balance in an NWP model from a large number of very short-range forecasts. The idea is that over a large number of forecasts the parametrised forcing and dynamical forcing should balance each other. Klinker and Sardesmukh found that the "residual" between the dynamic and parametrised tendencies bore a strong resemblance to the long term systematic error of the ECMWF model. They were then able to investigate contributions to this residual from the individual model routines such as convection or gravity wave drag. Some examples of applying this technique to the UM are given below. All calculations are carried using 210 two-timestep forecasts from the four UKMO analyses available every day between 12\1\95 and 6\3\1995

Diabatic Forcing

Figure 18(a) shows the parametrised diabatic heating applied to the model and consists of terms due to radiation, convection, boundary layer turbulent mixing, and large scale condensational heating due to evaporation of precipitation and formation/dissipation of layer cloud. There are heating maxima in the tropics, in the boundary layer from 60N to 60S, and in the extratropical mid-

troposphere. Significant cooling occurs in the subtropics above 900hPa which is radiative in origin (Fig. 19(d)) , and also at the tropopause and over the poles. Figure 18(b) shows the dynamical heating terms shown with their sign reversed for easier comparison with the diabatic heating. There is a great deal of similarity between the parametrised and (-)dynamical heating rates. If the model is in thermal balance then these two terms should be identical. The degree of imbalance is given by the total tendency (Fig. 18(c)) which is the sum of the parametrized and dynamical terms. The total tendency bears a remarkable resemblance to the zonally averaged T+72 temperature error (Fig. 9(c)).

We can split the thermal balance further by considering the contribution to the parametrised diabatic heating from the individual model routines (Fig. 19). The radiative terms (Fig 19(d)) are dominated by the LW cooling, with maxima at the tropopause, and subtropical boundary layer. The T+72 cold bias in the southern hemisphere boundary layer is clearly associated with excessive radiative cooling due to low cloud (Fig 19(e)). The warming in the tropical mid-troposphere may be due to excessive convective heating early in the forecasts. The radiative terms also appear to contribute to the cooling in the upper tropopause. Comparison with the ECMWF model (Klinker, personal communication) shows the upper troposphere radiative cooling rates are larger in the UM. The picture is more complex in local areas such as the NH stormtracks where the dynamics may also contribute to the upper tropospheric cold bias (see MOSAC paper P2 by Kershaw and Slingo, 1996 for more discussion). In the stratosphere the parametrised terms have smooth fields, whereas the dynamical fields are very noisy (Fig 18(b)) and dominate the residual tendency (Fig. 18(c)).

Momentum forcing

Figure 20 shows the zonally averaged zonal momentum balance for Jan/Feb/Mar 1995. Although the stratospheric GWD has been reduced since January 1995, it is possible that it may still be overdone (see -2m/s/day at 30N and level 16). Evidence for this comes from the dynamics tendencies (shown with sign reversed) at 40N and 200hPa which show westerly tendencies at the site of the applied GWD (30N-40N, 50hPa) and easterly tendencies below (Fig. 20(b)). This pattern is consistent with zonal wind tendencies that would be generated by a thermally direct (anticlockwise) meridional circulation in the upper troposphere. The hypothesis is that such a meridional circulation is generated in order to maintain geostrophic and hydrostatic balance in the presence of an excessive drag in the stratosphere. The impact of these dynamical adjustments is to cause a residual momentum tendency at 200hPa which *decellerates* the subtropical jet (Fig. 18(c)). In the boundary layer there is a residual westerly tendency in the extratropics and easterly tendency in the tropics which suggests a lack of parametrised drag. In the NH this westerly tendency is geographically located over the main orographic ranges. Again the residual tendencies are consistent with the model's sytematic error in

zonal wind (Fig. 1(b)). The dynamics terms also suggest of the need for a small drag on the easterlies in the tropical upper troposphere at 0N and 200hPa. Finally we note a large dynamical adjustment of the zonal wind field over Antarctica, the cause of which is currently not known.

3.6 Synoptic variability

So far we have only considered the time mean state of the atmosphere. In this section we consider the ability of the global UM to forecast synoptic variability in DJF on two different time scales, (i) 1-6 days and (ii) ~10 days. Associated with these timescales we consider cyclonic developments and blocking respectively.

Band Pass Filtered MSLP - Stormtracks

The band pass filter of Blackmon (1976) is applied to the MSLP analysis and T+120 forecasts for the period DJF 1994/95 to highlight variability in the 2-6 day timescale. The analysed stormtracks (Fig. 21(a)) have maxima in the Atlantic and Pacific ocean basins and over the eastern U.S and Canada. The T+120 forecast stormtracks (Fig. 21(b)) show a reduction in synoptic variability over the U.S., increased synoptic variability in the eastern ocean basins, and a more zonal orientation to the stormtracks. These errors in the stormtracks (see Fig. 21(c)) are consistent with the time mean errors in the upper tropospheric winds showing reductions in vertical shear in the jet entrances and extension of the jet core into the eastern ocean basins in the forecasts (Fig. 7).

Cyclonic Developments/Tracking - Baroclinic lifecycles.

The MSLP mean errors and the stormtrack variability suggest significant errors in representing the lifecycle of the baroclinic waves at longer forecast ranges. To investigate this further we have applied an objective cyclone tracking program developed at GSFC by Atlas and Terry to UM analyses and forecasts for DJF 94/95. This index gives us a central pressure and position (lat., long.) of each analysed and forecast low allowing objective validation of depth and position errors. A typical error in the lifecycle of a explosive extratropical cyclone is shown in Figure 22. During the deepening phase the forecasts underestimate the central pressure of the low, and in the filling phase the forecasts are all too deep by 5-10hPa. These errors in the lifecycle are consistent with the systematic errors in MSLP (Fig. 3(b)).

Blocking

We use the objective blocking index of Tibaldi and Molteni (1990) to assess the UM performance in comparison with the ECMWF model. In DJF 92/93 the UM showed a clear reduction

in the frequency of blocks in the Atlantic and Pacific at longer forecast ranges (Fig. 23). In contrast the ECMWF model has a more realistic blocking frequency. In DJF 95/96 the UM has a much improved blocking frequency at T+120, equivalent to that predicted by ECMWF. This improvement is thought to be largely due to the introduction of orographic roughness and a revised GWD scheme in January 1995, which reduced the zonalisation of the flow (Fig, 5). The UM still shows a tendency to shift the blocking maxima eastward compared to the analyses.

4. DEVELOPMENTS IN THE MESOSCALE MODEL AND LAM

Where the global model provides forecasts of large-scale synoptic development and upper level winds for aviation customers, the Mesoscale Model (MES) and Limited Area Model (LAM) are primarily used to provide detailed "weather" forecasts. An example of the performance of the MES and LAM in forecasting monthly precipitation accumulations in the forecast range 0-24 hours for January 1996 is shown in Figure 24. The verifying data is the station data accumulated into 5km grid squares for use in MORECS. Both models capture the broad scale distribution of precipitation over the UK. The MES clearly has more detail provided by its higher resolution orography and forecasts the maxima seen in MORECS over the Lake District, South Wales, and Dumfries and Galloway in Scotland. However the MES does show a tendency to overpredict the orographic precipitation over the Grampians and the Pennines. The MES also predicts the dry areas in the low lying regions better than the LAM, although both models have too much precipitaion over Central England

Changes in model formulation in the Mesoscale Model (MES) have kept pace with those in lower resolution configurations, in keeping with the 'Unified' model philosophy. For data assimilation, however, there has been a greater exploitation of data sources best suited to the higher resolution of the MES, particularly those giving information on the moisture field. The Moisture Observation Pre-processing System (MOPS), blends satellite imagery, surface cloud reports and radar imagery to produce a 3-dimensional cloud analysis for assimilation by the MES (Macpherson et al. 1996).

Initially, MOPS required interactive quality control by a forecaster for safe use of infrared imagery. Development of automatic cloud top height assignment algorithms for stratocumulus led to a fully automatic MOPS system in October 1993. During 1994, another problem with the use of infrared imagery became manifest, namely incorrect assignment of thin cirrus to medium levels, with consequent initiation of spurious convection in the model. The incidence of this was appreciably reduced by a prior quality control check on the model's high cloud background field, implemented in April 1995. A more complete solution will involve simultaneous use of infrared and water vapour imagery, and should be introduced early in 1997. Further exploitation of imagery data has seen a

Latent Heat Nudging scheme introduced (in April 1996) to assimilate radar based rain rate estimates, leading to improved MES precipitation distributions in the early stages of the forecast. The MOPS cloud analysis now also runs in 'large-area' mode for the Limited Area Model (LAM), with benefit in summertime thundery conditions, where analysis over the data sparse Bay of Biscay can be crucial (Fig. 25). Objective measurement of the benefit of observations to MES precipitation forecasts (by verification against radar data) shows that MOPS data now deliver significant benefit roughly as often as the radiosonde network.

Soil moisture content (smc) is important for determining mesoscale variations in near-surface temperature, especially on hot clear days. The MES smc initialisation has undergone major changes in successive years. In 1994, a climatological field was imposed, giving too moist a field in a dry summer, and a cool bias in temperature forecasts. In 1995, the MES smc was allowed to evolve freely during data assimilation, but a deficiency in analysed cloud led to excessive drying of the model and a marked warm bias on hot days. The excess drying (Fig. 26) was measured relative to an independent land-surface model (MORECS) run for agricultural customers, which has the benefit of observed sunshine amounts. This summer, 1996, a weekly MES smc initialisation has been performed from MORECS data. This has largely removed the warm bias on hot days, and leaves a cool bias in mid-afternoon temperatures, the origin of which seems to be at least partly linked with precipitation parametrization.

5. VERIFICATION

The global model has shown a steady improvement in accuracy. An example is the T+72 RMS errors in NH MSLP measured against UKMO analyses (Fig. 27). This decreased between 1992 and 1993/94 and with the introduction of orographic roughness and new GWD scheme in January 1995 both RMS error and model bias showed dramatic improvements in every month in 1995. The UM compares favourably against other centres in terms of accuracy measures. For example the 500hpa geopotential height RMS errors over Europe and North America measured against observations (Fig. 28) show improvements in the UM forecasts during winter in recent years (compare October-March 1993 with the same period in 1995/96).

Figure 29 shows the mean and RMS errors for surface temperature in the MES as measured against station data over the UK for April 1993 to September 1996. The problem with the drying of the land surface and too warm surface temperatures in JJA 1995 can be seen in the RMS errors verifying at both 06Z (Fig. 29(c)) and 12Z (Fig. 29(d)), and also in the 06Z mean errors (Fig. 29(a)). The temperature errors in JJA 1996 have been reduced with the resetting of soil moisture in the MES

assimilation. The RMS vector wind errors for the 10m winds have shown a steady decrease (Fig. 30(a)) with the changes to surface drag made through the orographic roughness (Appendix B).The mean errors in cloud cover (Fig 30(b)) have also been reduced since the beginning of 1995 and are now within ± 1 okta at T+24.

6. PLANNED IMPROVEMENTS TO MODEL FORMULATION

6.1 Autumn 1996 Package - Global Model.

Three major changes to the global model formulation have been approved for implementation in November 1996 .

- Fourth order advection
- Cumulus Momentum transports
- Gravity Wave drag Revisions

The fourth order advection has been used for a number of years in the climate version of the Unified Model and recent tests in the NWP versions have shown a beneficial impact on verification scores and a reduction in the systematic errors associated with the jets. The cumulus momentum transports have also been extensively tested in climate simulations and NWP forecasts and shown to dramatically improve the tropical simulation. Following information from the momentum balance diagnostics and sensitivity studies the gravity wave drag scheme has been modified to extract less drag in the stratosphere. A further change will be made in November 1996 to include the 1DVAR assimilation of TOVS radiances for the moisture field in the assimilation. Amongst other things this improves the tropical simulation, removing some of the spurious precipitation maxima in the east tropical Pacific.

6.2 High resolution tests - Global Model

With the arrival of the CRAY T3E supercomputer the plan for 1997 is to increase horizontal resolution from 90km to 60km and the vertical levels from 19 to 30. Preliminary tests of this configuration have shown a beneficial impact on wind scores. A parallel trial of increased horizontal resolution also showed a improvements in the forecast of Hurricane Bertha (Fig. 31)

There are also plans in 1997 to replace the LAM and MES with a 10km mesocale model operating on a larger domain than the current MES, which would rationalise the current operational suite from 3 to 2 models.

7. SUMMARY

The Unified Model (UM) has shown a steady improvement in performance since its introduction in 1991. The largest improvement in the global model came with the revisions to orog raphic forcing in January 1995. This reduced RMS errors, reduced the zonalisation of the flow and improved blocking in the model. The change to fourth order moisture diffusion (March 1993) and the revisions to moisture assimilation (November 1994) were both reduced the model spinup in moisture and reduced the lower tropospheric cold bias. Large uncertainties still remain over the veracity of analysed and forecast moisture fields in the UM, particularly in the upper troposphere. The numerous other model changes have had less dramatic effects, but their signature can still be detected in model improvements. For example, the removal of the warm bias in the lower tropical troposphere with the introduction of convective downdraughts.

Outstanding problems in the global UM are the cold bias, the moist bias, the extratropical westerly bias (largest in the SH), and errors in jet structure. Many NWP models and GCM's suffer from similar systematic errors. A list of the outstanding errors in the global UM are given in Appendix C.

The LAM and Mesoscale (MES) models have undergone similar formulation changes to the global model. The biggest improvements in precipitation forecasts have been through the assimilation of additional data sources for moisture. A cloud analysis (MOPS) has been introduced in MES and LAM with beneficial impact in summer thundery conditons for systems moving from data sparse areas such as the Bay of Biscay. A latent heat nudging scheme in the MES to assimilate radar rain estimates leads to improved precipitation distributions early in the forecast range. Finally, a weekly initialisation of soil moisture to values given by an independent land surface model (MORECS) have alleviated the drying and warming in the model during the summer months.

Acknowledgments.

Thanks to Anette Van der Wal for providing many of the global model diagnostics and Bruce Macpherson and Byron Chalcraft for the material on the Mesoscale and LAM. Verification statistics courtesy of Frank Saunders and Ed Dargan.

8. REFERENCES

Barkstrom, B.R.,1988: The Earth Radiation Budget Experiment (ERBE). *Bull.Am. Meteor.Soc.,65,1170-1185*

Blackmon, M.L., 1976: A climatological spectral study of the 500mb geopotential height in the Northern Hemisphere. *J.Atmos. Sci, 40,1410-1425.*

Cullen, M.J.P., 1993: The Unified Model. *The Meteorological Magazine, 122, 81-94*

Jaeger,L., 1976 : Monthly precipitation maps for the entire earth. *Bericht Deutscher Wetterdienst 18 Nr 139, 38pp*

Kershaw, R. and A. Slingo., 1996: Results from the cold bias project. (Paper for MOSAC meeting 11/12 November 1996).

Klinker, E. and P.D.Sardesmukh, 1992: The diagnosis of mechanichal dissipation in the atmosphere from large scale balance requirements. *JAS, 49,608-627.*

Macpherson B., Wright B.W., Hand W.H. and Maycock A.J. 1996 The impact of MOPS moisture data in the UK Meteorological Office data assimilation scheme. Mon. Weath. Rev. 124, 2023-2045.

Milton, S.F. and C.Wilson, 1996: The impact of parametrized subgridscale orographic forcing on systematic errors in a global NWP model. Mon. Weath. Rev. 124, 1746-1766.

Rossow,W.B. and R.A.Schiffer, 1991:ISCCP Cloud Data Products.*Bull.Am. Meteor.Soc.,72,2-20*

Slingo, A. and J.M. Slingo, 1988: The response of a GCM to cloud longwave radiative forcing. I Introduction and initial experiments. *Q.J. Meteorol. Soc., 114, 1027-1062.*

Tibaldi, S. and F. Molteni, 1990: On the operational predictability of blocking. Tellus, 42A, 343-365.

Warren, S.G., C.J.Hahn, and J.London, 1985: Simultaneous occurrence of different cloud types. *J.Climate Appl. Meteor., 24, 658-667.*

Appendix A - Changes to Global Model Formulation 1991-1996

12 November 1991	Horizontal diffusion of humidity changed from 4th to 2nd order
24 March 1992	Implement vertical diffusion in tropics
7 April 1992	Introduce ECMWF-like LW transmissivities.
9 March 1993	1) Horizontal diffusion of humidity changed from 2nd to 4th order. 2) Correct error in position of orographic standard deviation for GWD calculation. 3) Correct 2nd order term in vertical advection calculation.
3 August 1993	Introduction of ERS-1 scatterometer winds into the assimilation.
11 January 1994	2nd Climate Version Physics (HadAM2a) introduced into the global model (1) Include downdraughts in convection scheme. (2) Introduce rapidly mixing boundary layer. (3) Layer clouds in 3 layers for SW (4) Random overlap replaced by Max/Random overlap in LW (5) Revision of evaporation rates for snow. (6) Threshold for precipitation over sea reduced.
12 April 1994	Change to global assimilation to balance surface pressure and temperature increments using wind increments (WINDBAL)
10 October 1994	New tropical cyclone bogussing
29 November 1994	Humidity fix to radiosondes in LAM and global models. (1) Revised processing of radiosonde humidity (replacing vertical by interpolation to midpoint and introducing a boost near saturation) (2) Revised humidity assimilation (to conserve RH during T update)
13 December 1994	(1) Long physics timesteps for both global and LAM models- global model has 3 physics timesteps per hour compared with 6 for the dynamics. (2) Code in both models to prevent superadiabatic profiles from being generated.
10 January 1995	New Gravity wave drag and orographic roughness in global and LAM models.
20 June 1995	Switch off of horizontal diffusion over steep orography.
16 January 1996	3rd Climate Version Physics (HADAM2b) introduced into the global model (1) Mixed phase cloud now -9 to 0 degC compared to -15 to 0 degC (2) More accurate qsat. (3) Cloud water distribution used for precipitation formation. (4) Modified ice-fallout (5) Correct boundary layer height +double asymptotic mixing length (global & LAM) (6) MRF/UMIST effective radious water drops (global)
16 January 1996	New orographic roughness fields (global & LAM)
16 April 1996	Introduce GLobal Sounding System (GLOSS - 1DVAR assimilation of TOVS radiances)

Appendix B - Changes to the Mesoscale Model Formulation 1993-1996

14 September 1993	Del4 diffusion.
	Standard Convective Closure Parameters.
	2nd Climate Version Physics (Hadam2a)
	Convection Every other Timestep (cost saving).
	New Fog and Cloud Diagnostics
	Screen level RH assimilation and revised assimilation parameters
5 October 1993	Automatic MOPS.
2 November 1993	Increased vertical resolution. Extra bottom level. Revised critical RH profile.
8 December 1993	Rain evaporation correction.Spurious Snow showers correction.
23 August 1994	Continuous Assimilation. Four runs a day.
27 September 1994	New assimilation parameters. Correction to sonde data in cloud.
	New treatment of drag over orography. Minor changes to physics.
	Assimilation of rainfall to correct soil moisture.
	Aerosol predicted to feed into visibility diagnostic.
	Long physics timestep.
4 April 1995	MOPS changed to output cloud not RH.
11 April 1995	Revised orographic roughness scheme.
	More intelligent diffusion.
	Improved screen Temperature interpolation.
	MOPs improvement.
	New Assimilation parameters (esp winds).
	Assimilation of visibility for visibilty forecasts.
	Free running soil moisture content with rainfall assimilation.
16 January 1996	3rd Climate Version Physics (Hadam2b).
	Negative q local correction.
	Changes to precipitation scheme.
	Modified diffusion around steep orography.
	Correction to boundary layer code.
	Correction to specification of saturation humidity mixing ratio.
16 April 1996	Latent Heat Nudging scheme introduced.
22 May 1996	Soil moisture now reset to MORECS values each Wednesday
4 June 1996	Change from IBM to Nimrod version of MOPS.
23 July 1996	Much improved land use data.

Appendix C - Outstanding Systematic Errors in the Global Model.

Tropopause cooling (Tropics and Extratropics)

Cold bias in NH winter oceanic stormtracks throughout the depth of the troposphere.

SH stormtrack cooling

Warming in the tropical mid troposphere.

Nightime temperatures too low over continents in winter.

Subtropical jets -reduction of speed in jet cores, reduction of vertical wind shear

Extratropical westerly bias

Easterlies too intense in upper tropical troposphere (reduced with cumulus momentum transports)

Overactive tropical divergent circulation(reduced with cumulus momentum transports)

Spin up in cloud and precipitation in extratropical stormtracks

Spin down in tropical precipitation.

Moist bias.

Top of the atmosphere Planetary Albedo too large / SWCF too large.

Top of the atmosphere OLR too large./LWCF too small.

Top of the atmosphere Clear sky OLR too large.

Top of the atmosphere Clear sky albedos too small.

Baroclinic lifecycle is incorrect - lows too shallow in deepening phase and too deep in mature phase.

Blocking frequency has improved. Still a tendency for Atlantic blocks to shift eastward.

Figure Captions

Figure 1: Zonally averaged height latitude cross sections for December, January, February 95/96 of a) Analysed zonal wind (m/s), b) T+72 zonal wind error, c) and d) as a) and b) but for June, July and August, 1995.

Figure 2: Zonally averaged height latitude cross sections for December, January, February 95/96 of a) Analysed meridional wind (m/s), c) T+72 meridional wind error, b) and d) as a) and c) but for June, July and August, 1995.

Figure 3: Mean sea level pressure for December, January, February 95/96; a) Analysed at 00Z , b) T+72 mean error.

Figure 4: Mean sea level pressure for June, July and August 1995; a) Analysed at 00Z , b) T+72 mean error.

Figure 5: Time latitude diagram of zonally averaged T+72 mean sea level pressure errors from June 1991 to July 1996.

Figure 6: 500hPa geopotential height for December, January, February 95/96; a) Analysed at 00Z , b) T+72 mean error.

Figure 7: Northern Hemisphere zonal wind at 250hPa for December, January, February 95/96; a) Analysed at 00Z , b) T+72 mean error.

Figure 8: Results of sensitivity experiment (GWDSEN) to remove stratospheric gravity wave drag from the Unified Model (see text for details). a) Analysis of zonal wind at 70hPa, b) Operational forecast T+72 mean error, c) Impact of sensitivity experiment on 70hPa zonal wind at T+72 (GWDSEN - Operational), c) GWDSEN mean error at T+72.

Figure 9: Zonally averaged height latitude cross sections for December, January, February 95/96 of a) Analysed temperature, c) T+72 temperature error, b) and d) as a) and c) but for June, July and August, 1995.

Figure 10: T+72 mean temperature error at a) 850hPa for January 1995, b) 250hPa for January 1995, c) 850hPa for July 1994, d) 250 hPa for December, January, February 95/96.

Figure 11: Time latitude diagram of zonally averaged T+72 mean error in temperature from October 1992 to July 1996, a) 850hPa, b) 300hPa.

Figure 12: Time series (June 1991- Feb 1995) of monthly mean a) Precipitation -evaporation b) Global average precipitation.

Figure 13: Tropical precipitation for a) Unified Model T+00 to T+24 December 1994, b) Unified Model T+48 to T+72 December 1994, c) GOES Precipitation Index (see text) for December 1994, d) Jaeger climatology for December, e) Legates and Willmott climatology for December.

Figure 14: Time latitude diagram of zonally averaged T+72-T+00 mean difference in relative humidity from August 1991 to October 1995 at 850hPa.

Figure 15: Monthly mean, zonally averaged total cloud amount for the Unified Model, ISCCP and Warren

et. al. climatology (see text for details) for a) January and b) August.

Figure 16: LW cloud forcing (TOA) in Watts per metre squared for a) Unified Model during January 1995, b) ERBE during January 1988, c) UM - ERBE.

Figure 17: SW cloud forcing (TOA) in Watts per metre squared for a) Unified Model during January 1995, b) ERBE during January 1988, c) UM - ERBE.

Figure 18: Monthly mean thermal balance in the Unified Model for January/February/March 1995. a) Parametrized heating rates (K/day) - Diabatic component, b) Dynamical heating rates (adiabatic component) with sign reversed, c) Total (residual) tendency = Parametrizations + Dynamics.

Figure 19: Contributions to monthly mean thermal balance for January/February/March 1995 from the individual parametrized terms a) Total radiation (SW+LW), b) Convection, c) Boundary layer turbulent mixing, d) Large scale condensation (Clouds and precipitation). Units are K/day. Also shown is e) Layer cloud fraction (zonally averaged).

Figure 20: Monthly mean, zonally averaged zonal momentum balance in the Unified Model for January/February/March 1995. a) Parametrized drag , b) Dynamical tendencie s with sign reversed ("implied" drag), c) Total (residual) tendency = Parametrizations + Dynamics. Units are m/s/day.

Figure 21: Band pass (2-6 days) filtered standard deviation of MSLP fields for DJF 94/95 for a) Analyses, b) T+120 forecasts c) T+120 mean error in band pass filtered standard deviation of MSLP.

Figure 22: Central pressures for deep Atlantic cyclone event from.

Figure 23: Frequency of blocked days in DJF 92/93 for a) UKMO, b) ECMWF and c) and d) as a) and b), but forDJF 95/96.

Figure 24: Precipitation accumulation for January 1996 for a) MORECS b) LAM at forecast range 0-24, c) Mesoscale model at forecast range 0-24. Units are mm.

Figure 25: Case study of the impact of MOPS in the LAM. T+18 forecasts are shown valid at 00z on 20/6/96 for a) Operational LAM, b) Trial LAM with MOPS included, c) Radar rainfall rate at 00Z 20/6/96.

Figure 26: Soil moisture content during 1995 for the operational free-running MES model, compared with MORECS and model climatology. The smc is normalised by capacity. Values are plotted as domain averages over the model and MORECS domains.

Figure 27: Time series of T+72 monthly averaged verification scores for mean-sea level pressure over the Northern Hemisphere domain (90N-30N). Verification is against UKMO analyses:a) RMS error, b) mean error.

Figure 28: 500hPa RMS errors calculated against upper air observations for a) European stations, b) North American Stations.

Figure 29: Verification of surface temperatures for the mesoscale model against surface station data from April 1993 to September 1996. a) Mean errors verifying at 06Z, b) Mean errors verifying at 12Z, c) RMS errors verifying at 06Z ands d) RMS errors verifying at 12Z.

Figure 30: Verification of near surface elements in the mesoscale model showing a) RMS vector wind errors verifying at 06Z and b) Mean cloud cover errors verifying at 06Z.

Figure 31 Hurricane Bertha - High resolution tests. All charts valid at 12Z 12/07/96 showing MSLP for a) Operational (90km) verifying analysis, b) Trial (60km) verifying analysis, c) Operational (90km) T+72 forecast, d) Trial (60km) T+72 forecast.

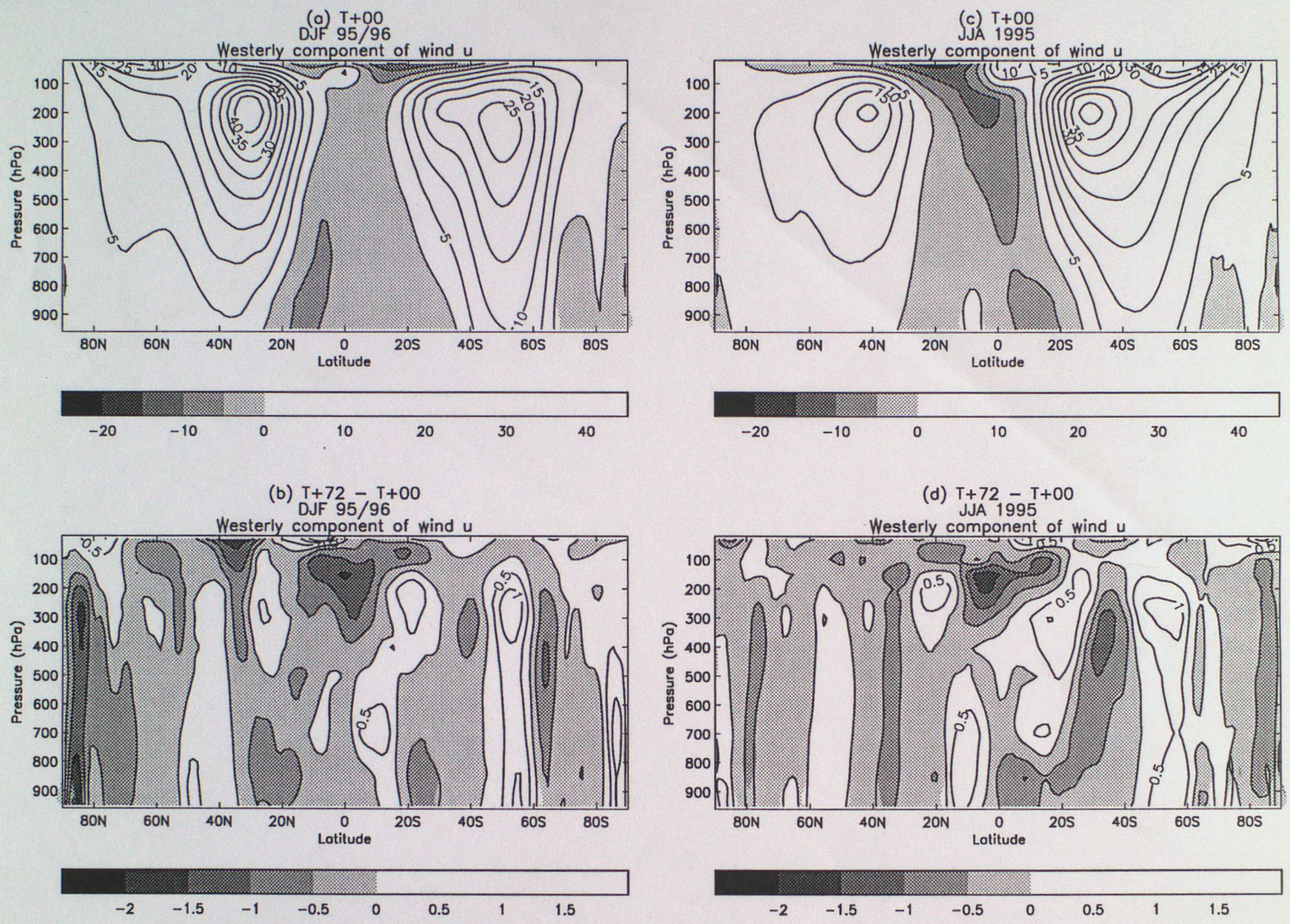
(a) T+00
DJF 95/96
Westerly component of wind u
(c) T+00
JJA 1995
Westerly component of wind u
(b) T+72 − T+00
DJF 95/96
Westerly component of wind u
(d) T+72 − T+00
JJA 1995
Westerly component of wind u
Pressure (hPa)
100
200
300
400
500
600
700
800
900
80N
60N
40N
20N
0
20S
40S
60S
80S
Latitude
−20
−10
0
10
20
30
40
−2
−1.5
−1
−0.5
0
0.5
1
1.5

Figure 1

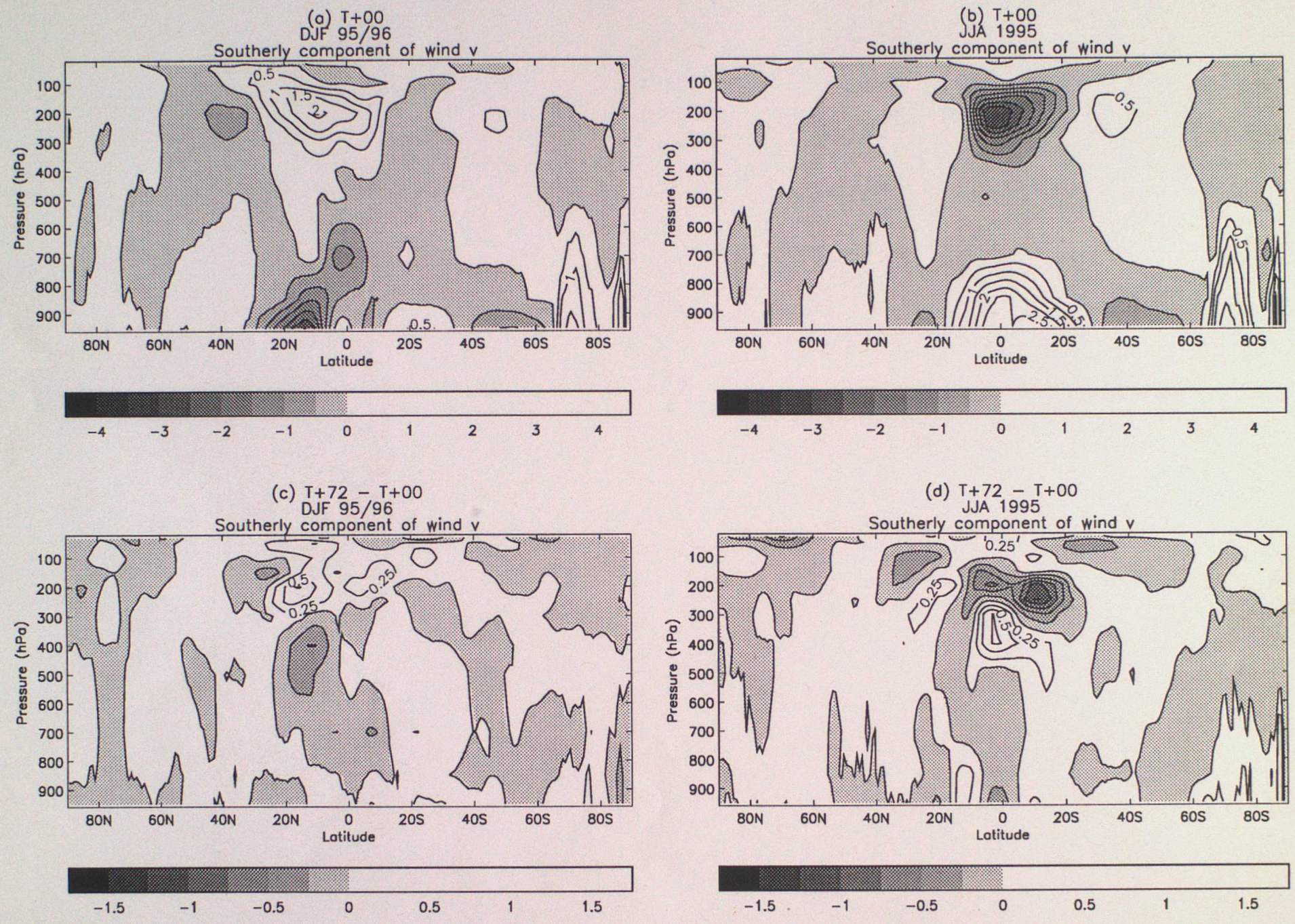
(a) T+00
DJF 95/96
Southerly component of wind v
(b) T+00
JJA 1995
Southerly component of wind v
(c) T+72 – T+00
DJF 95/96
Southerly component of wind v
(d) T+72 – T+00
JJA 1995
Southerly component of wind v
Pressure (hPa)
Latitude
80N 60N 40N 20N 0 20S 40S 60S 80S
100 200 300 400 500 600 700 800 900
−4 −3 −2 −1 0 1 2 3 4
−1.5 −1 −0.5 0 0.5 1 1.5

Figure 2

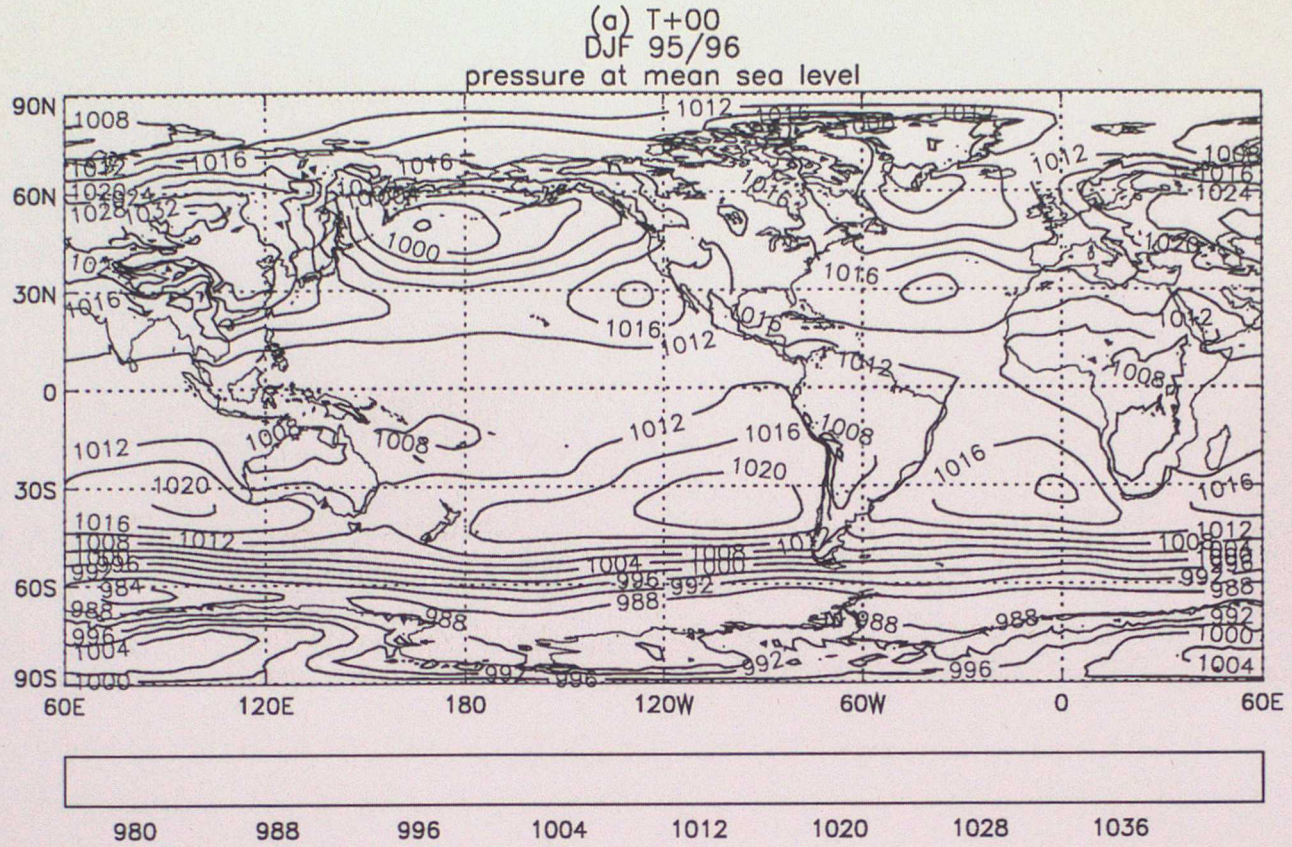
(a) T+00
DJF 95/96
pressure at mean sea level
90N
60N
30N
0
30S
60S
90S
60E
120E
180
120W
60W
0
60E
980
988
996
1004
1012
1020
1028
1036

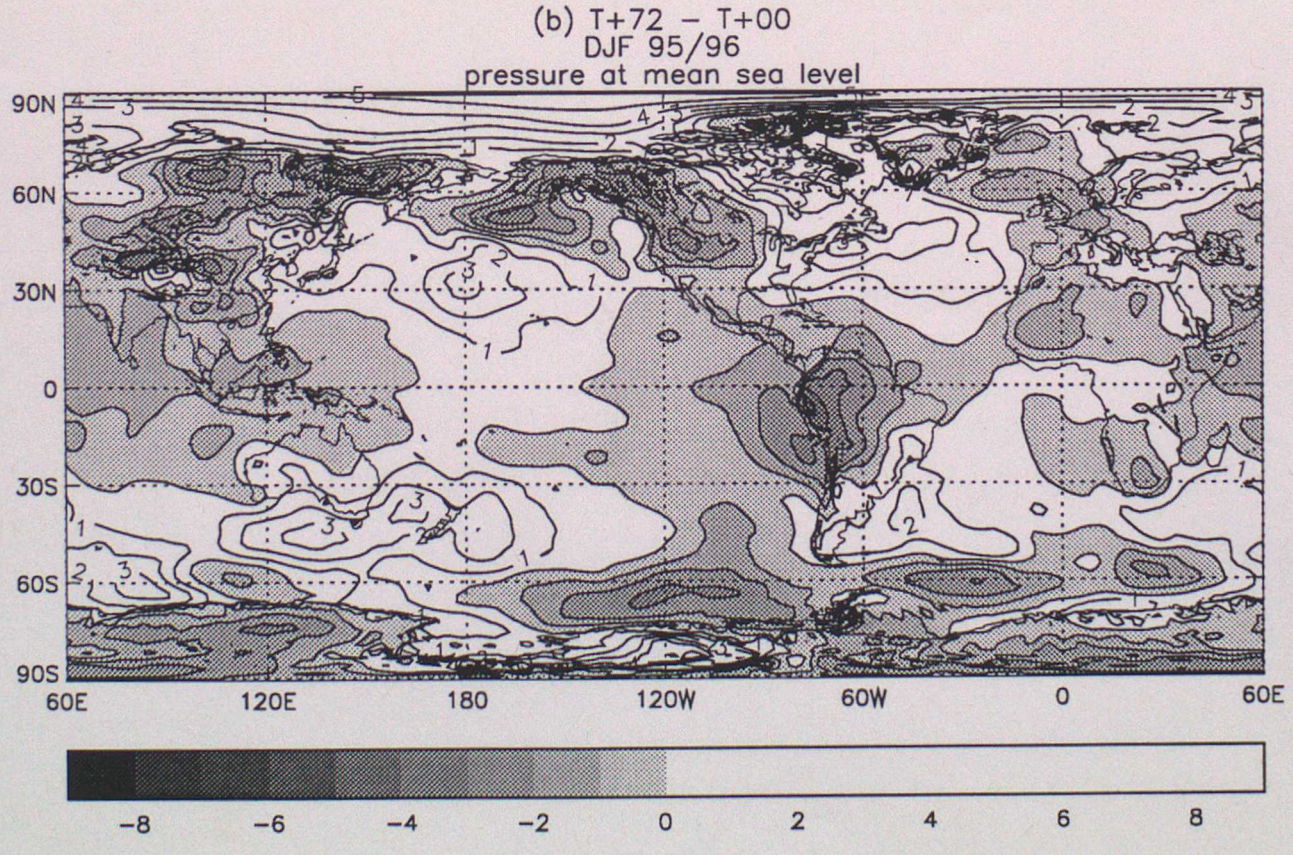
(b) T+72 – T+00
DJF 95/96
pressure at mean sea level
90N
60N
30N
0
30S
60S
90S
60E
120E
180
120W
60W
0
60E
−8
−6
−4
−2
0
2
4
6
8

Figure 3

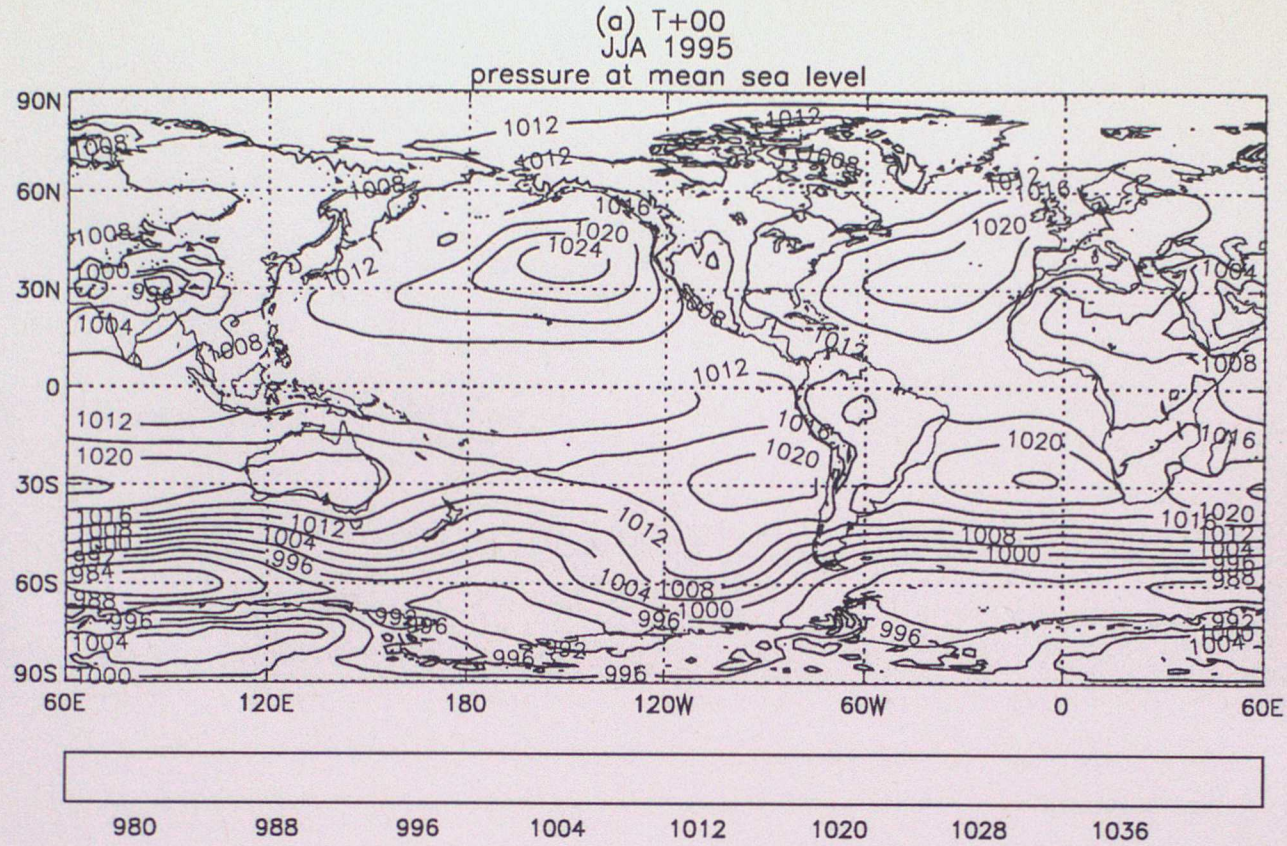
(a) T+00
JJA 1995
pressure at mean sea level
90N
60N
30N
0
30S
60S
90S
60E
120E
180
120W
60W
0
60E
980
988
996
1004
1012
1020
1028
1036

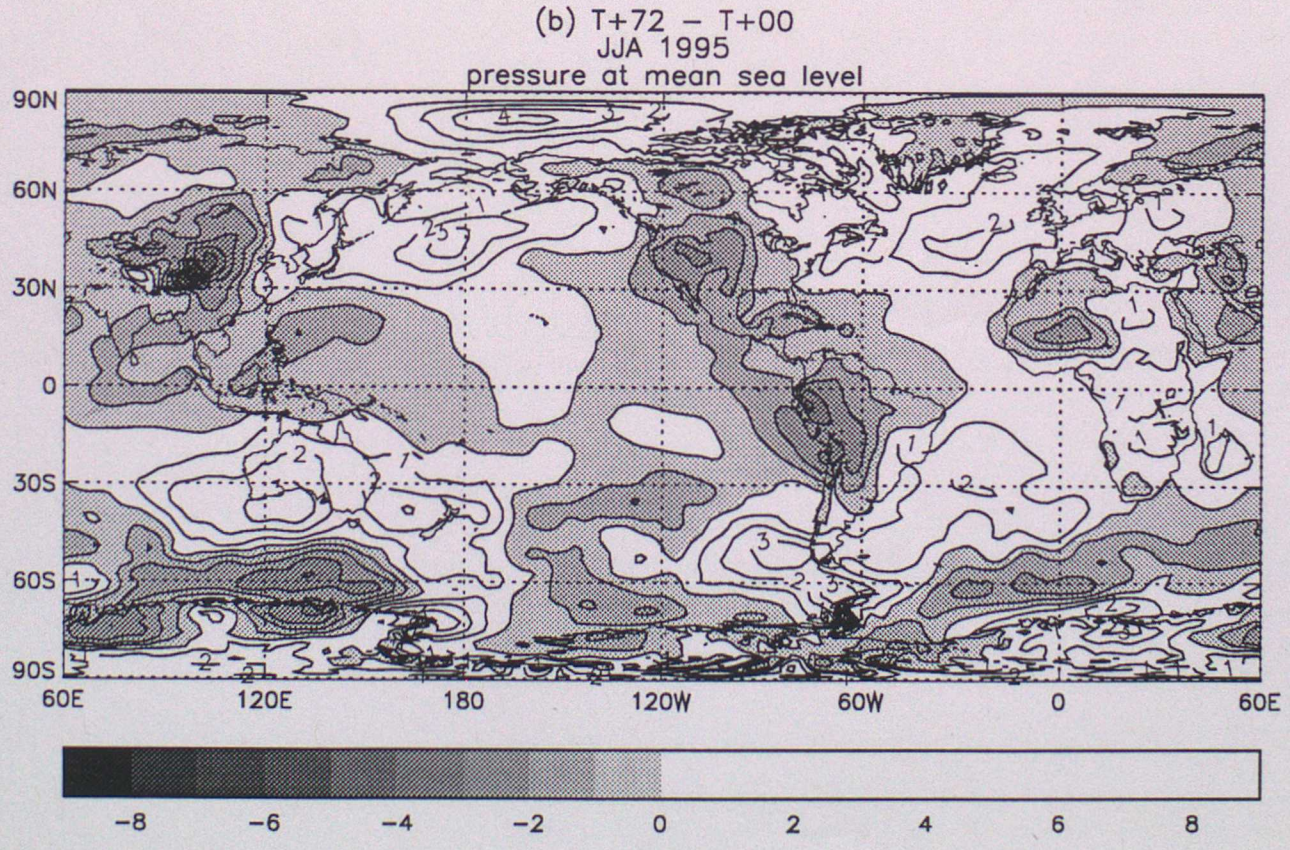
(b) T+72 – T+00
JJA 1995
pressure at mean sea level
90N
60N
30N
0
30S
60S
90S
60E
120E
180
120W
60W
0
60E
−8
−6
−4
−2
0
2
4
6
8

Figure 4

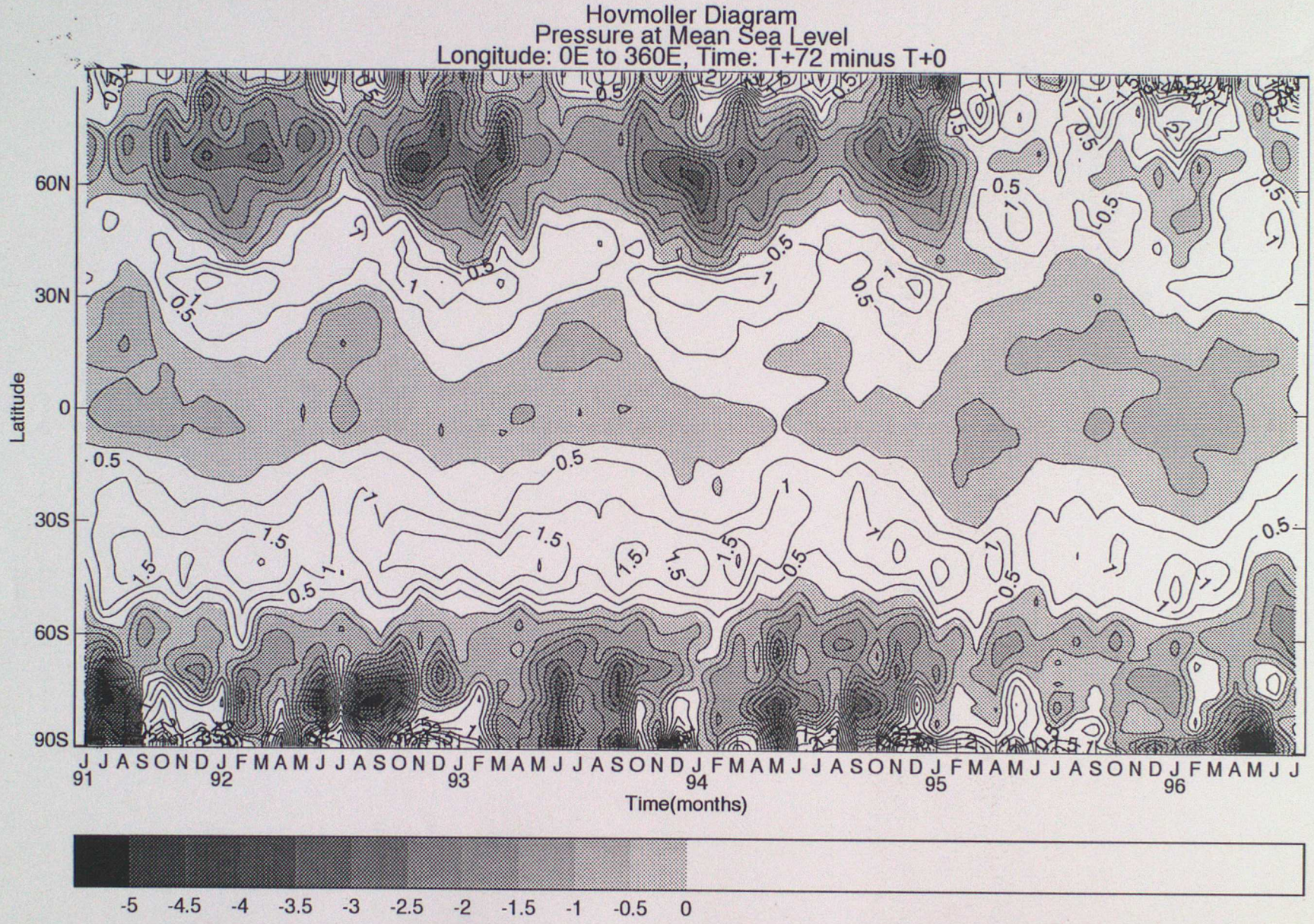
Hovmoller Diagram
Pressure at Mean Sea Level
Longitude: 0E to 360E, Time: T+72 minus T+0
Latitude
60N
30N
0
30S
60S
90S
J J A S O N D J F M A M J J A S O N D J F M A M J J A S O N D J F M A M J J A S O N D J F M A M J J
91
92
93
94
95
96
Time(months)
-5 -4.5 -4 -3.5 -3 -2.5 -2 -1.5 -1 -0.5 0

Figure 5

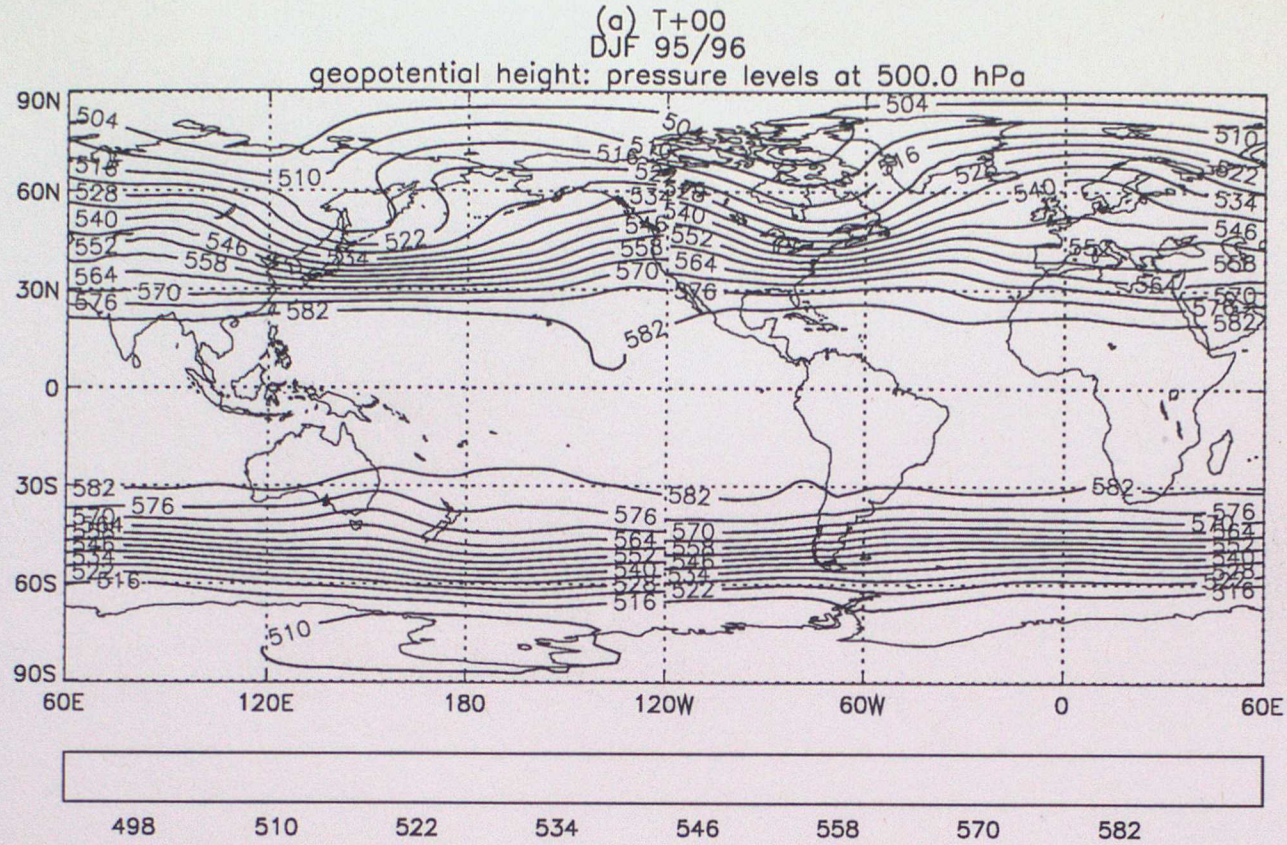
(a) T+00
DJF 95/96
geopotential height: pressure levels at 500.0 hPa
90N
60N
30N
0
30S
60S
90S
60E
120E
180
120W
60W
0
60E
498
510
522
534
546
558
570
582

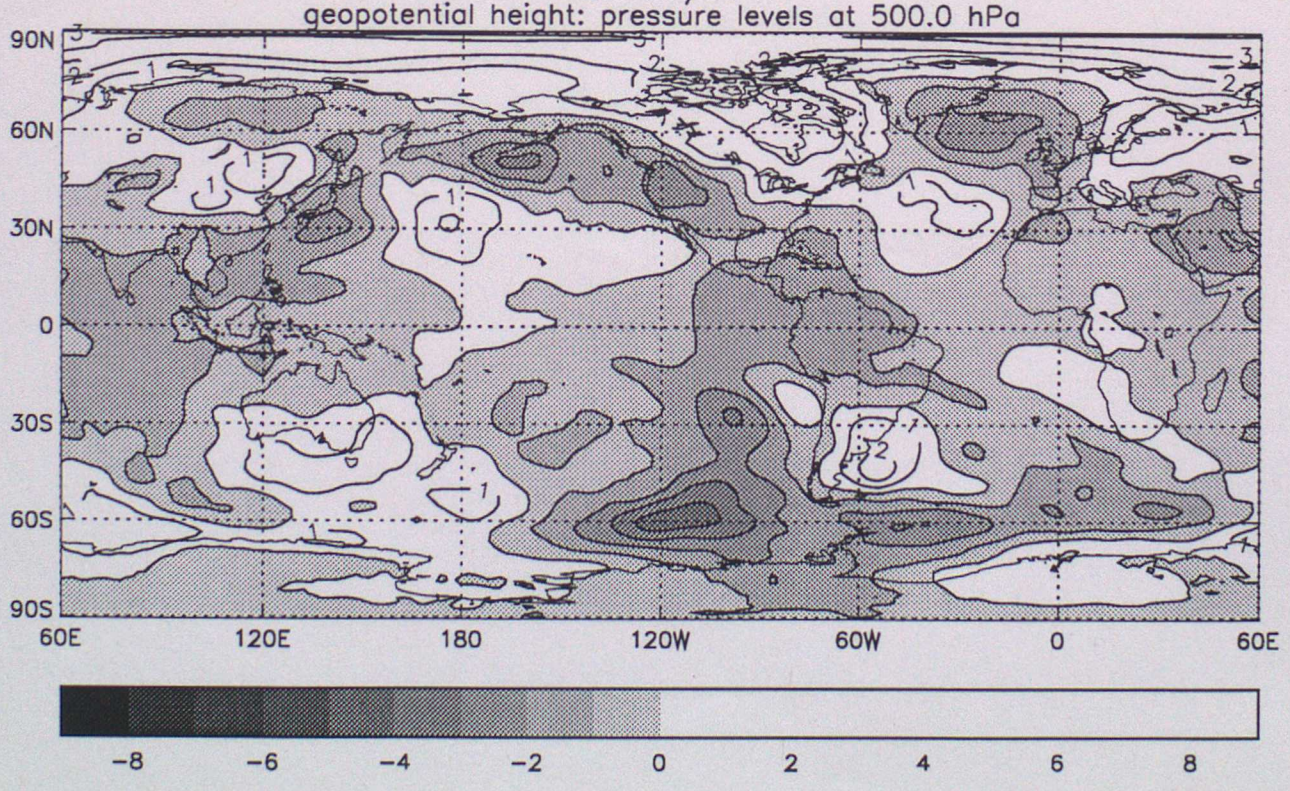
(b) T+72 − T+00
DJF 95/96
geopotential height: pressure levels at 500.0 hPa
90N
60N
30N
0
30S
60S
90S
60E
120E
180
120W
60W
0
60E
−8
−6
−4
−2
0
2
4
6
8

Figure 6

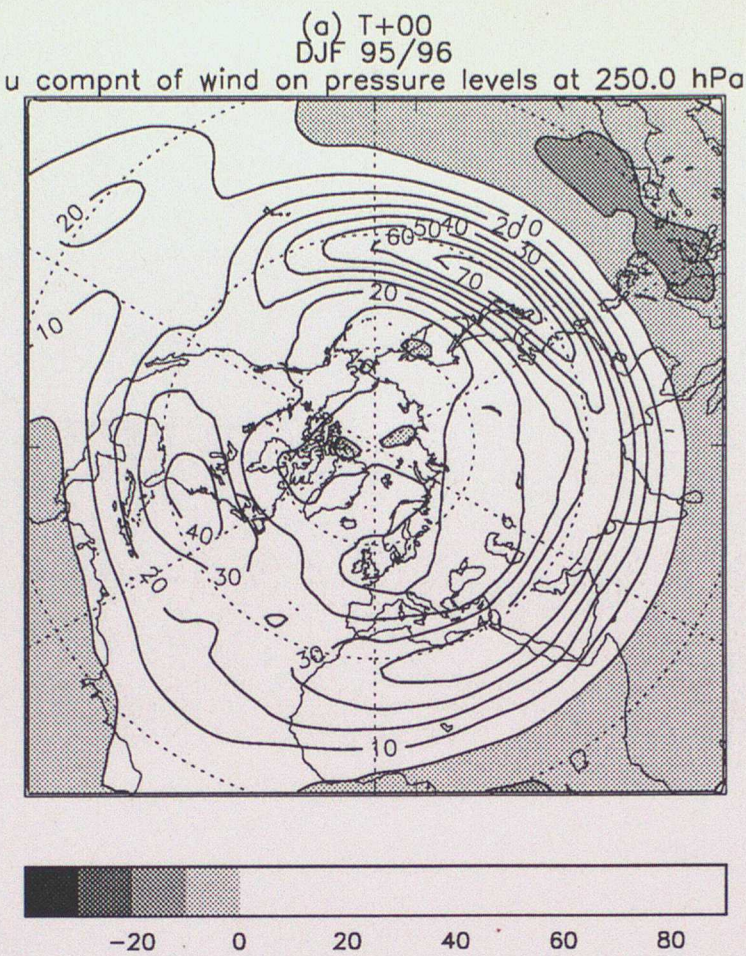
(a) T+00
DJF 95/96
u compnt of wind on pressure levels at 250.0 hPa
20
10
60
50
40
30
20
70
40
30
20
30
10
−20
0
20
40
60
80


(b) T+72 − T+00
DJF 95/96
u compnt of wind on pressure levels at 250.0 hPa
−8
−4
0
4
8

Figure 7

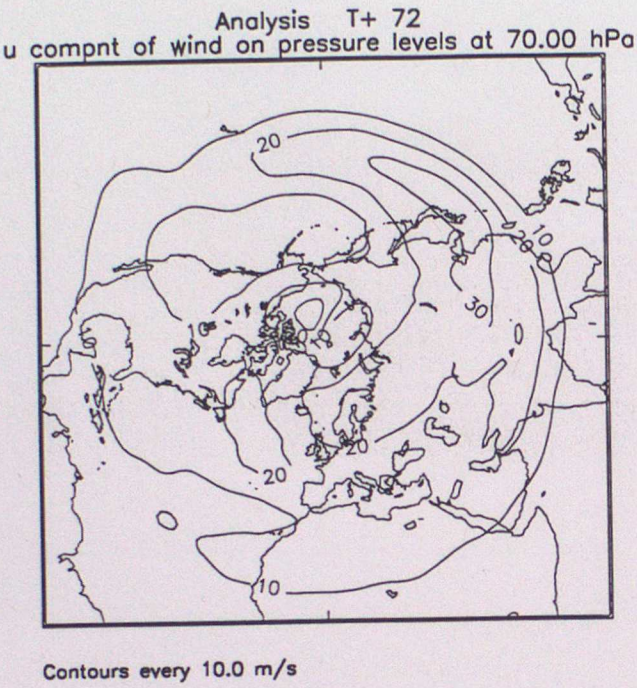
Analysis T+ 72
u compnt of wind on pressure levels at 70.00 hPa
20
10
30
20
20
10
Contours every 10.0 m/s

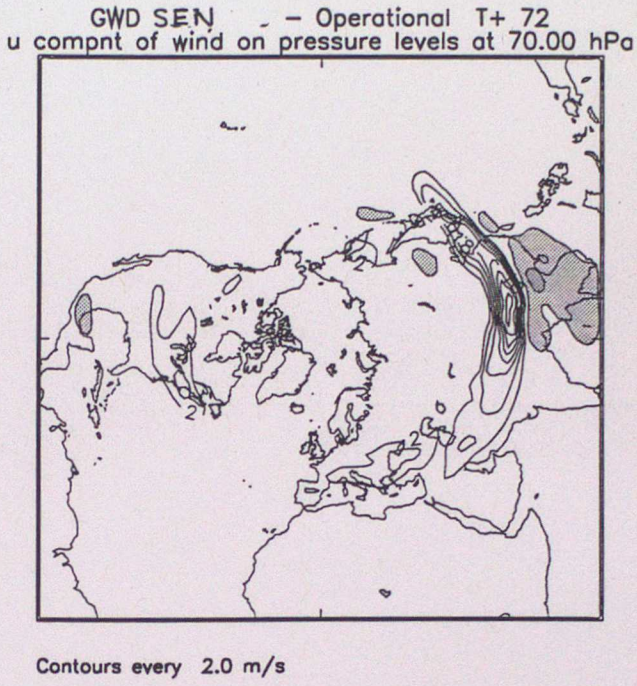
GWD SEN - Operational T+ 72
u compnt of wind on pressure levels at 70.00 hPa
2
2
2
Contours every 2.0 m/s

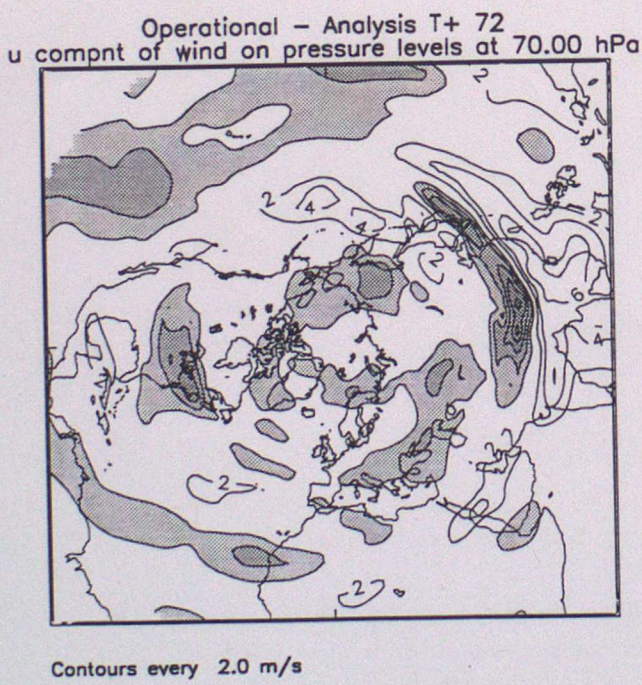
Operational - Analysis T+ 72
u compnt of wind on pressure levels at 70.00 hPa
2
2
4
4
2
2
2
2
Contours every 2.0 m/s

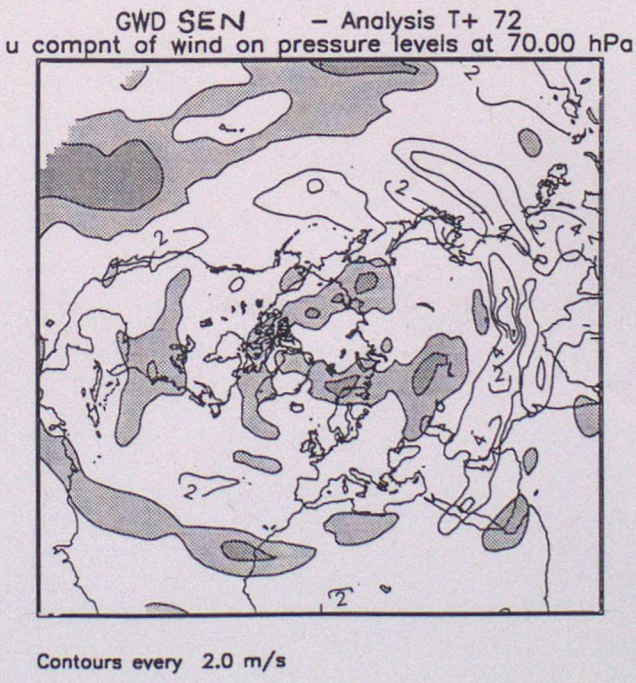
GWD SEN - Analysis T+ 72
u compnt of wind on pressure levels at 70.00 hPa
2
2
2
2
2
2
Contours every 2.0 m/s

Figure 8

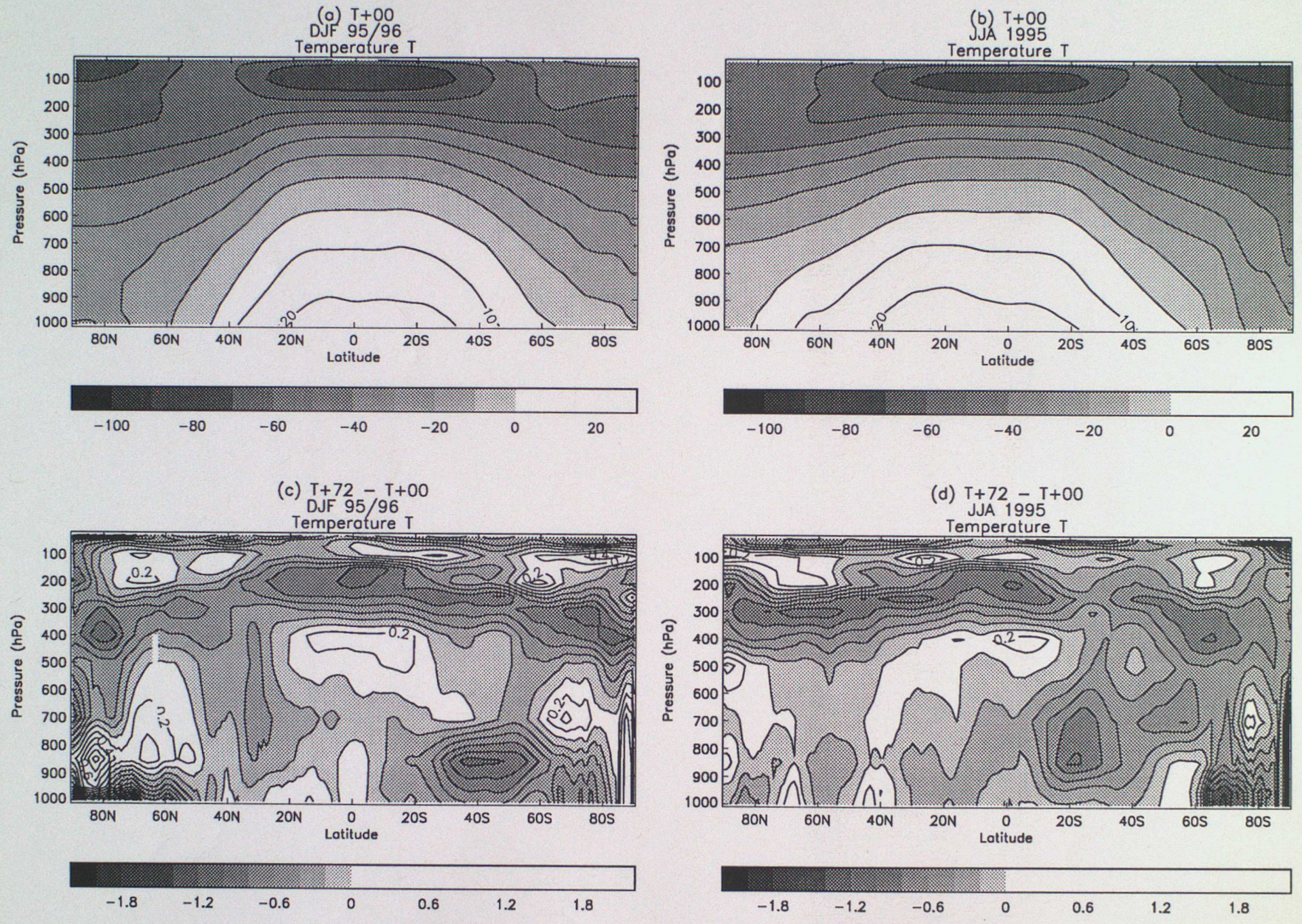
(a) T+00
DJF 95/96
Temperature T
(b) T+00
JJA 1995
Temperature T
(c) T+72 – T+00
DJF 95/96
Temperature T
(d) T+72 – T+00
JJA 1995
Temperature T
Pressure (hPa)
100
200
300
400
500
600
700
800
900
1000
80N
60N
40N
20N
0
20S
40S
60S
80S
Latitude
-20
-10
0.2
−100
−80
−60
−40
−20
0
20
−1.8
−1.2
−0.6
0.6
1.2
1.8

Figure 9

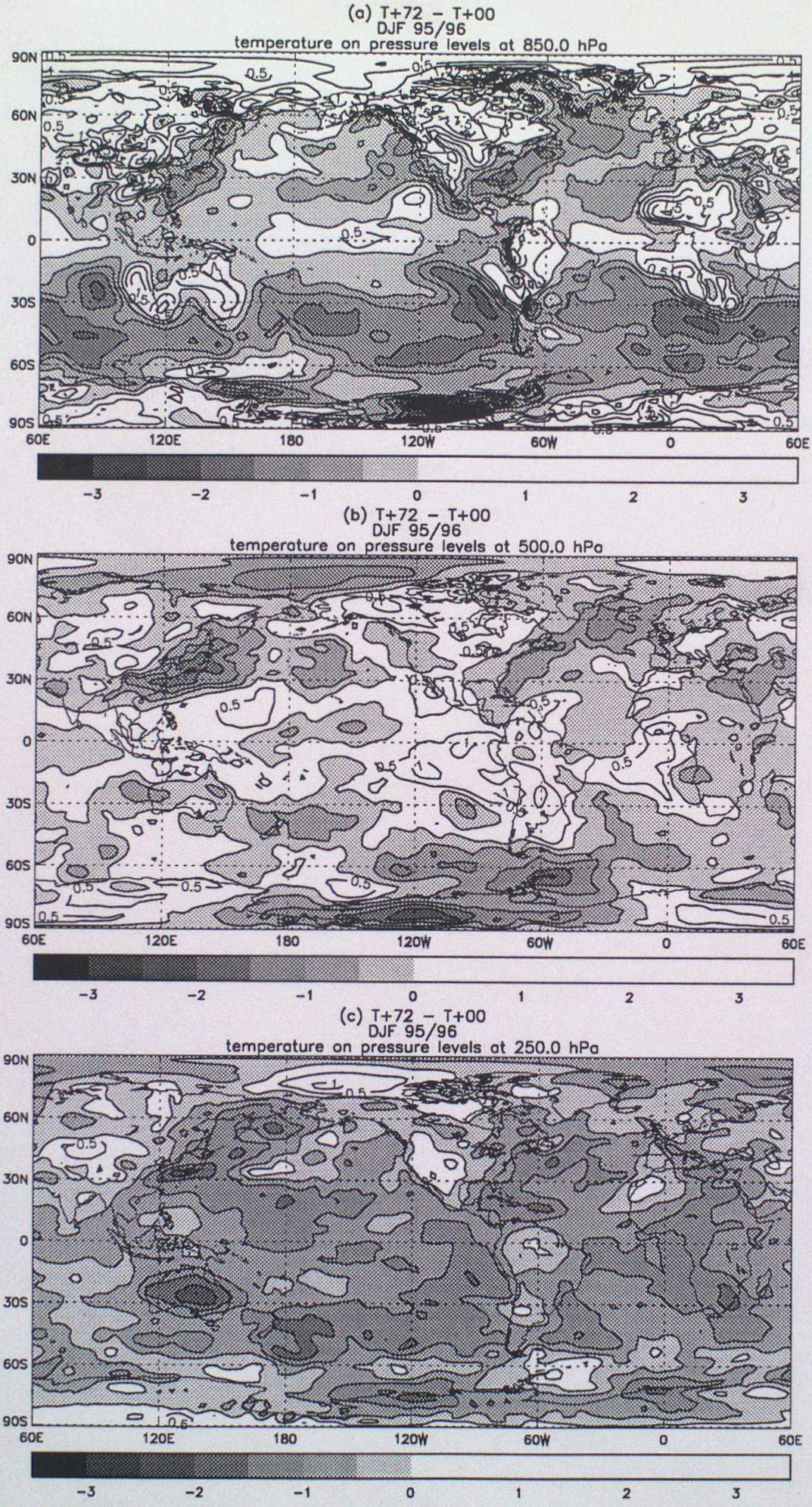
(a) T+72 – T+00
DJF 95/96
temperature on pressure levels at 850.0 hPa
90N
60N
30N
0
30S
60S
90S
60E
120E
180
120W
60W
0
60E
-3
-2
-1
0
1
2
3
(b) T+72 – T+00
DJF 95/96
temperature on pressure levels at 500.0 hPa
90N
60N
30N
0
30S
60S
90S
60E
120E
180
120W
60W
0
60E
-3
-2
-1
0
1
2
3
(c) T+72 – T+00
DJF 95/96
temperature on pressure levels at 250.0 hPa
90N
60N
30N
0
30S
60S
90S
60E
120E
180
120W
60W
0
60E
-3
-2
-1
0
1
2
3

Figure 10

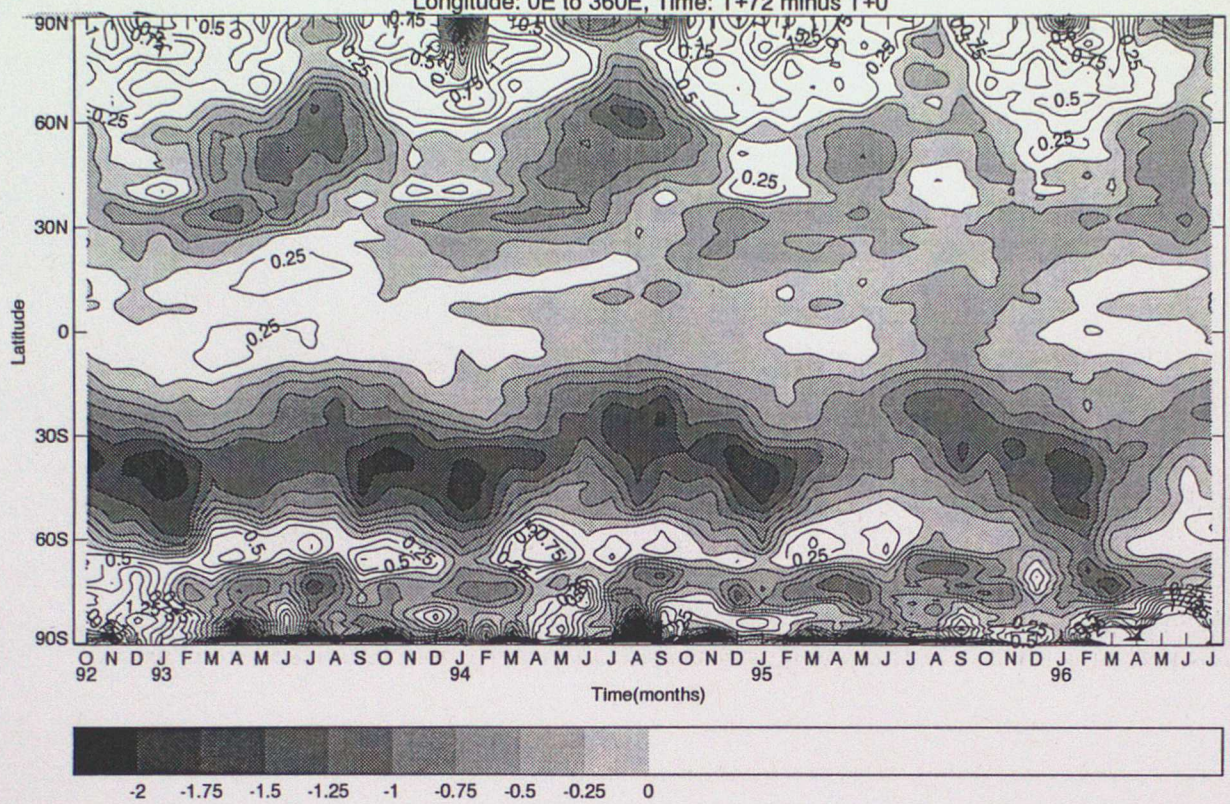
Hovmoller Diagram
Temperature at 850mb
Longitude: 0E to 360E, Time: T+72 minus T+0
90N
60N
30N
0
30S
60S
90S
Latitude
O N D J F M A M J J A S O N D J F M A M J J A S O N D J F M A M J J A S O N D J F M A M J J
92
93
94
95
96
Time(months)
-2 -1.75 -1.5 -1.25 -1 -0.75 -0.5 -0.25 0

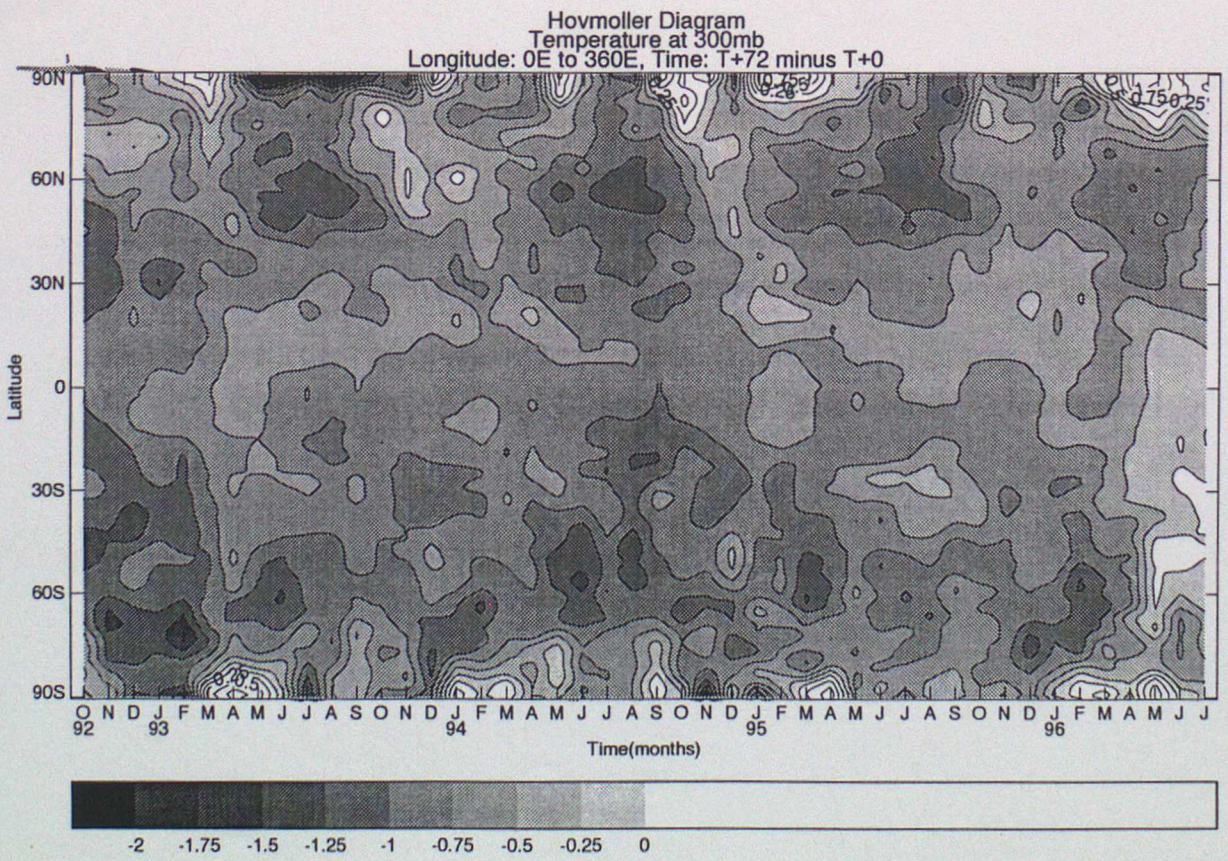
Hovmoller Diagram
Temperature at 300mb
Longitude: 0E to 360E, Time: T+72 minus T+0
90N
60N
30N
0
30S
60S
90S
Latitude
O N D J F M A M J J A S O N D J F M A M J J A S O N D J F M A M J J A S O N D J F M A M J J
92
93
94
95
96
Time(months)
-2 -1.75 -1.5 -1.25 -1 -0.75 -0.5 -0.25 0

Figure 11

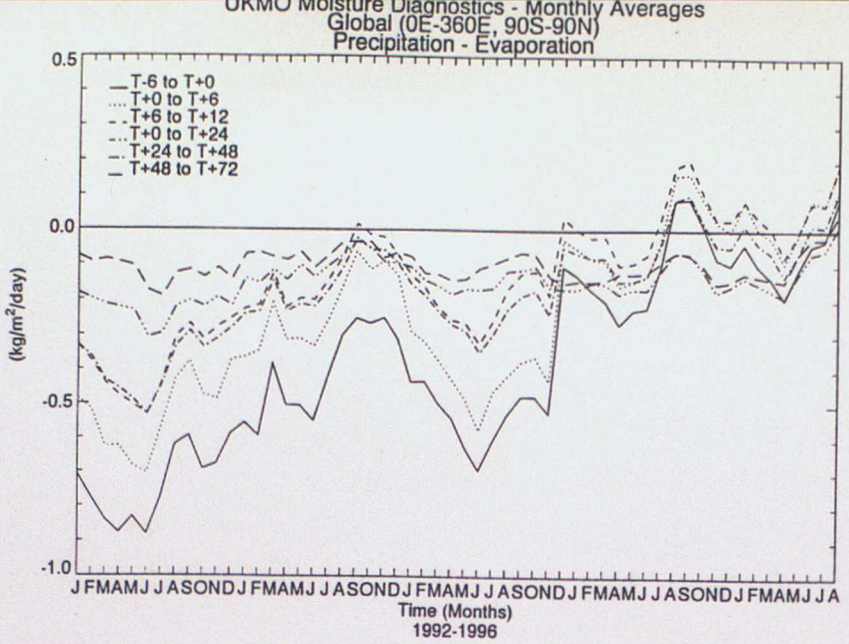
UKMO Moisture Diagnostics - Monthly Averages
Global (0E-360E, 90S-90N)
Precipitation - Evaporation
T-6 to T+0
T+0 to T+6
T+6 to T+12
T+0 to T+24
T+24 to T+48
T+48 to T+72
0.5
0.0
-0.5
-1.0
(kg/m²/day)
J FMAMJ J ASONDJ FMAMJ J ASONDJ FMAMJ J ASONDJ FMAMJ J ASONDJ FMAMJ J A
Time (Months)
1992-1996

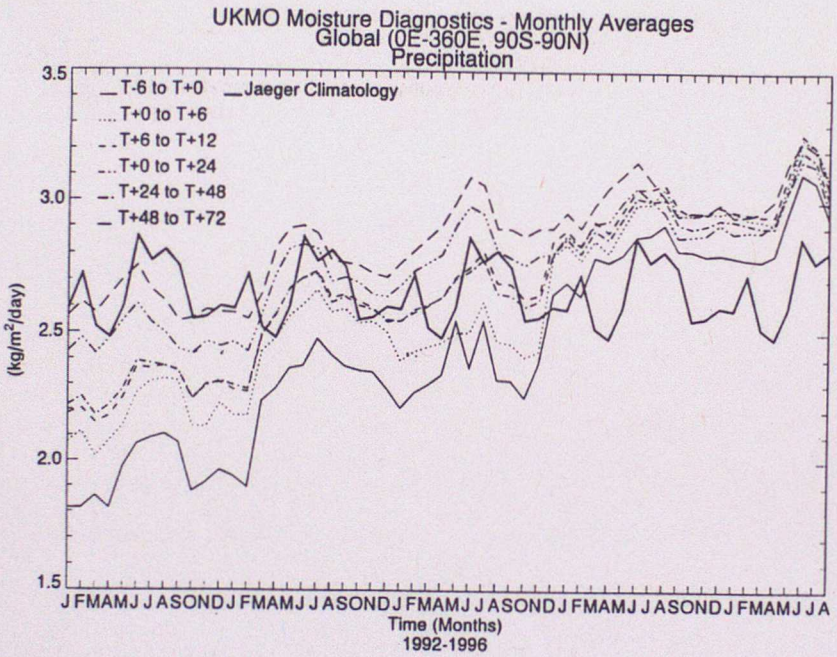
UKMO Moisture Diagnostics - Monthly Averages
Global (0E-360E, 90S-90N)
Precipitation
T-6 to T+0
Jaeger Climatology
T+0 to T+6
T+6 to T+12
T+0 to T+24
T+24 to T+48
T+48 to T+72
3.5
3.0
2.5
2.0
1.5
(kg/m²/day)
J FMAMJ J ASONDJ FMAMJ J ASONDJ FMAMJ J ASONDJ FMAMJ J ASONDJ FMAMJ J A
Time (Months)
1992-1996

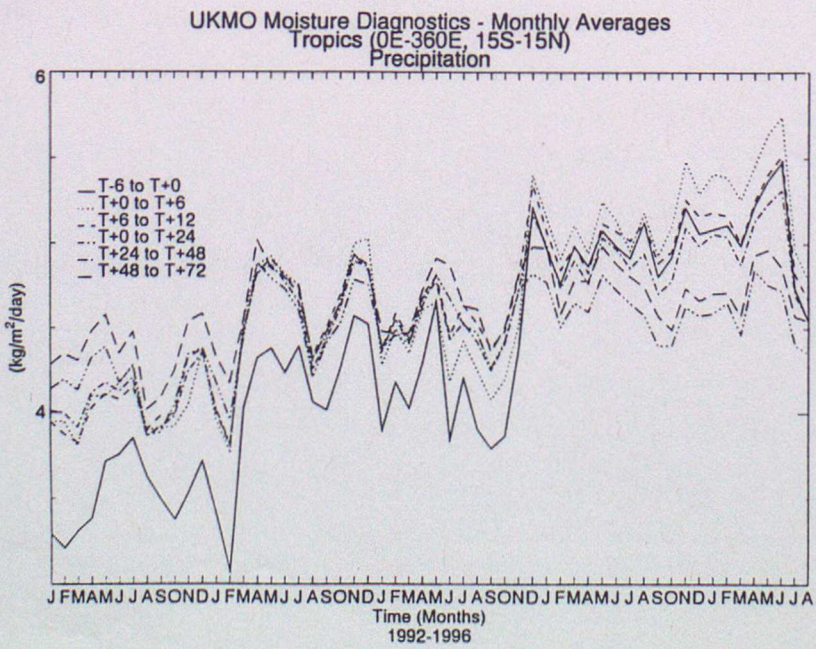
UKMO Moisture Diagnostics - Monthly Averages
Tropics (0E-360E, 15S-15N)
Precipitation
T-6 to T+0
T+0 to T+6
T+6 to T+12
T+0 to T+24
T+24 to T+48
T+48 to T+72
6
4
(kg/m²/day)
J FMAMJ J ASONDJ FMAMJ J ASONDJ FMAMJ J ASONDJ FMAMJ J ASONDJ FMAMJ J A
Time (Months)
1992-1996

Figure 12

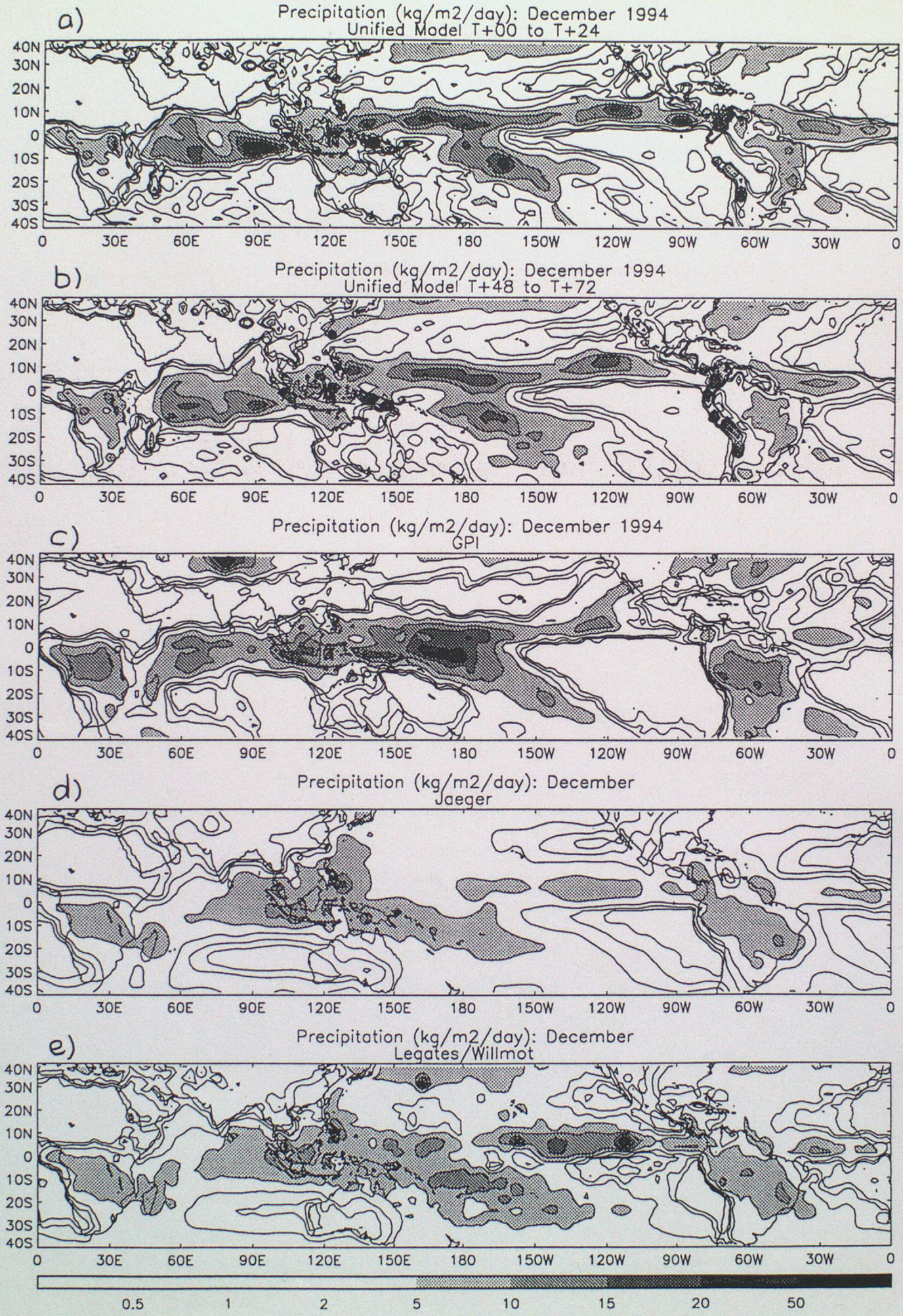
a)
Precipitation (kg/m2/day): December 1994
Unified Model T+00 to T+24
b)
Precipitation (kg/m2/day): December 1994
Unified Model T+48 to T+72
c)
Precipitation (kg/m2/day): December 1994
GPI
d)
Precipitation (kg/m2/day): December
Jaeger
e)
Precipitation (kg/m2/day): December
Legates/Willmot
40N
30N
20N
10N
0
10S
20S
30S
40S
0
30E
60E
90E
120E
150E
180
150W
120W
90W
60W
30W
0.5
1
2
5
10
15
20
50

Figure 13

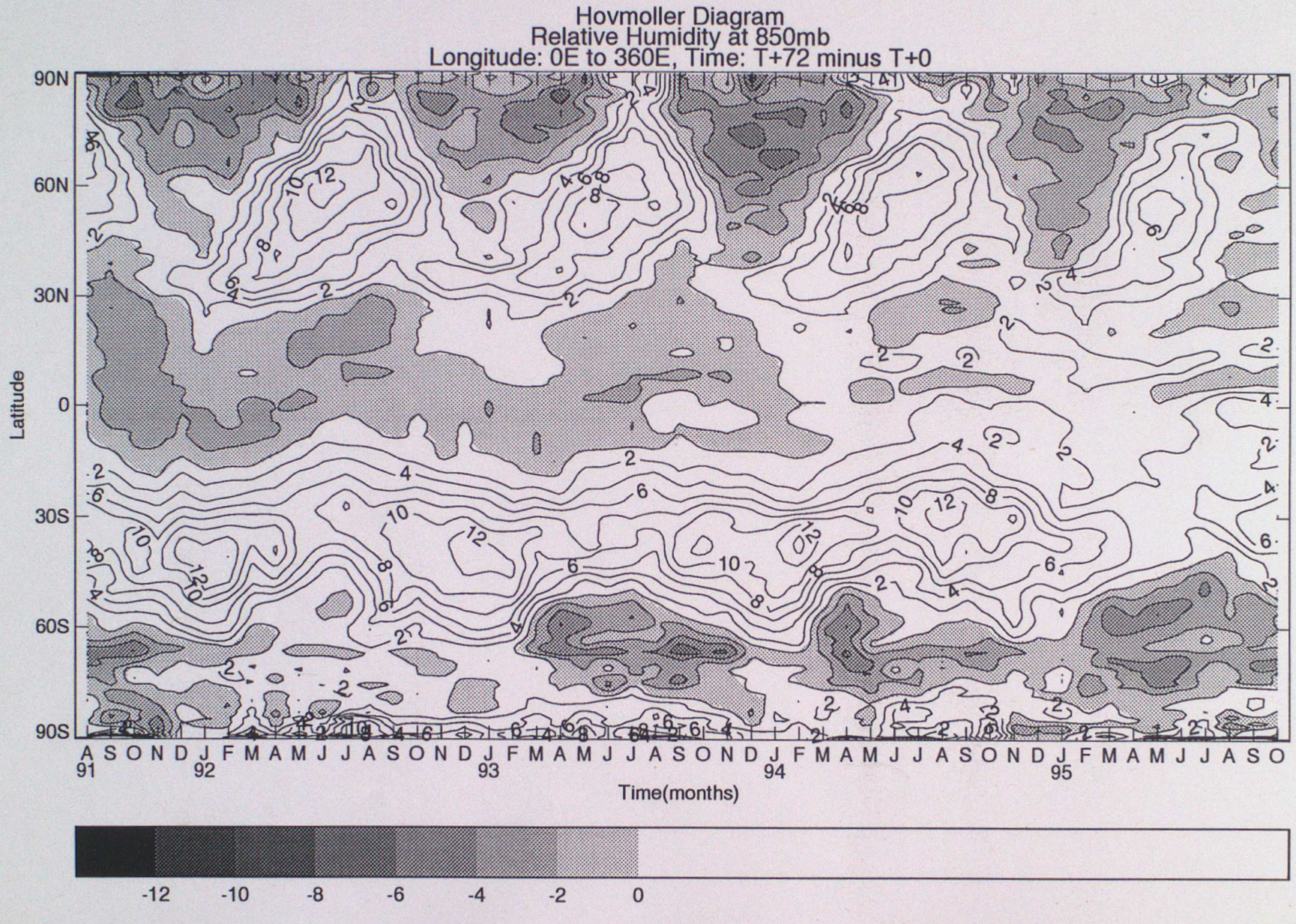
Hovmoller Diagram
Relative Humidity at 850mb
Longitude: 0E to 360E, Time: T+72 minus T+0
90N
60N
30N
0
30S
60S
90S
Latitude
A S O N D J F M A M J J A S O N D J F M A M J J A S O N D J F M A M J J A S O N D J F M A M J J A S O
91
92
93
94
95
Time(months)
-12
-10
-8
-6
-4
-2
0

Figure 14

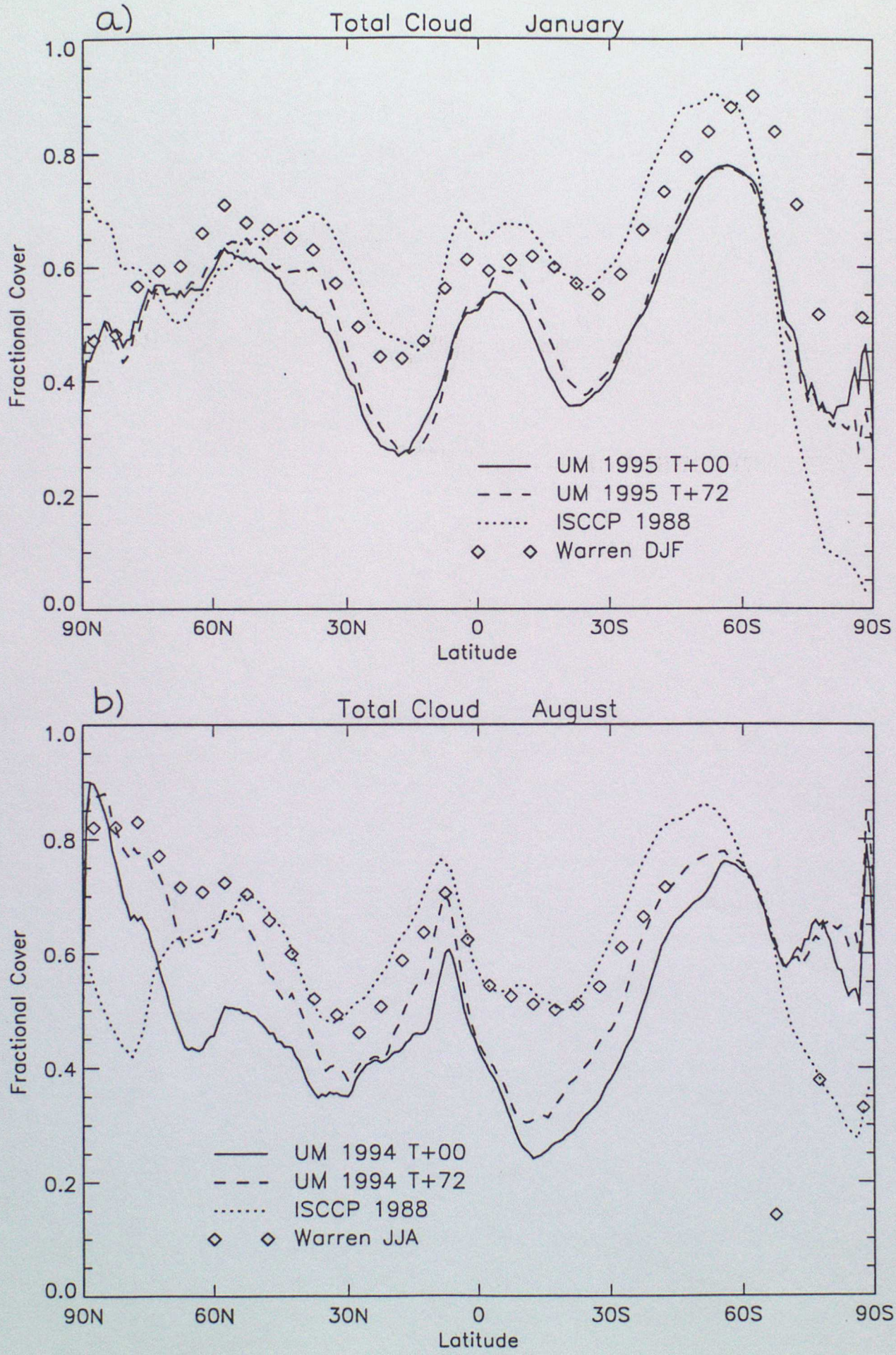
a)
Total Cloud January
1.0
0.8
0.6
0.4
0.2
0.0
Fractional Cover
UM 1995 T+00
UM 1995 T+72
ISCCP 1988
Warren DJF
90N
60N
30N
0
30S
60S
90S
Latitude
b)
Total Cloud August
1.0
0.8
0.6
0.4
0.2
0.0
Fractional Cover
UM 1994 T+00
UM 1994 T+72
ISCCP 1988
Warren JJA
90N
60N
30N
0
30S
60S
90S
Latitude

Figure 15

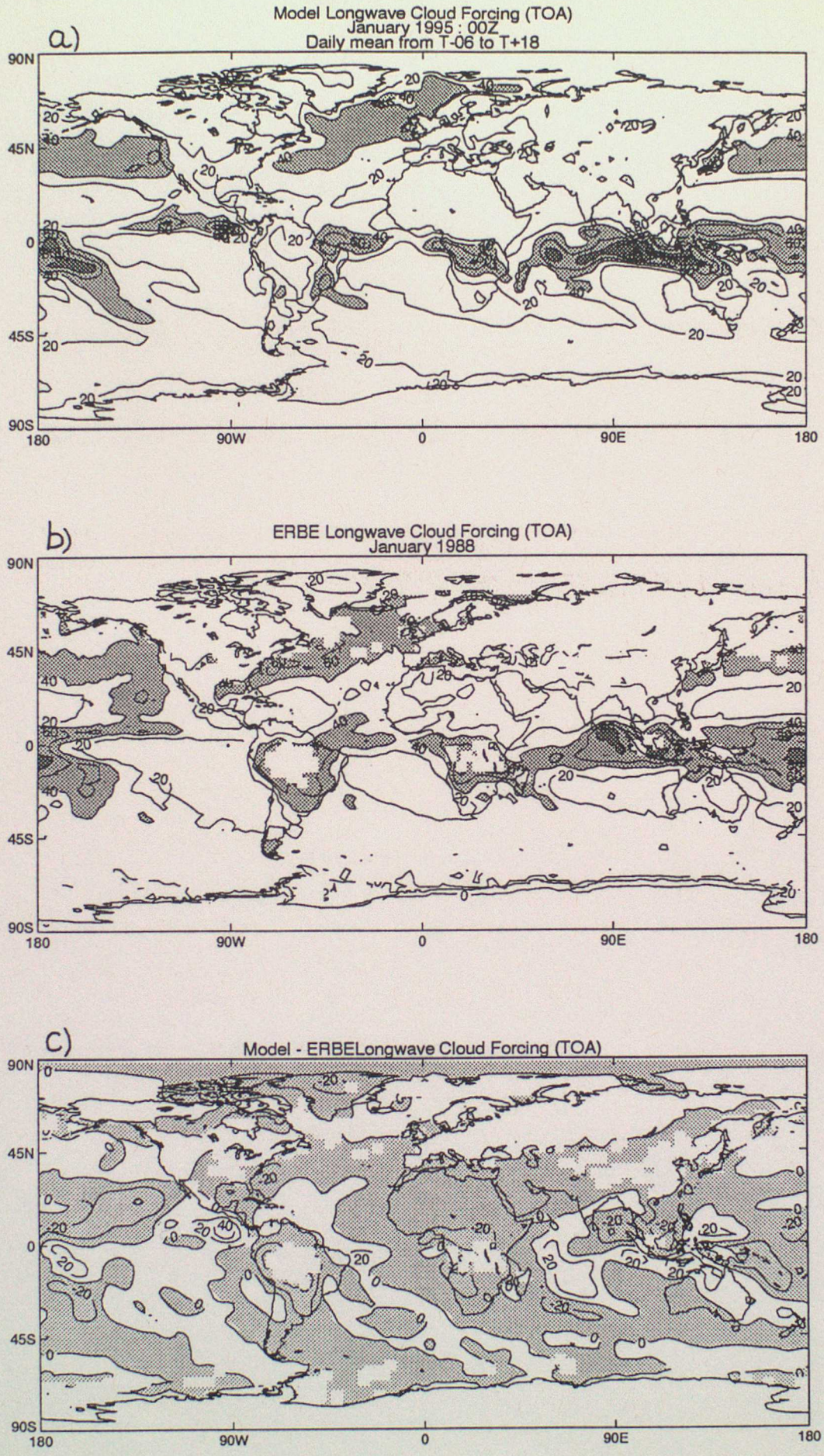
a)
Model Longwave Cloud Forcing (TOA)
January 1995 : 00Z
Daily mean from T-06 to T+18
b)
ERBE Longwave Cloud Forcing (TOA)
January 1988
c)
Model - ERBELongwave Cloud Forcing (TOA)
90N
45N
0
45S
90S
180
90W
0
90E
180

Figure 16

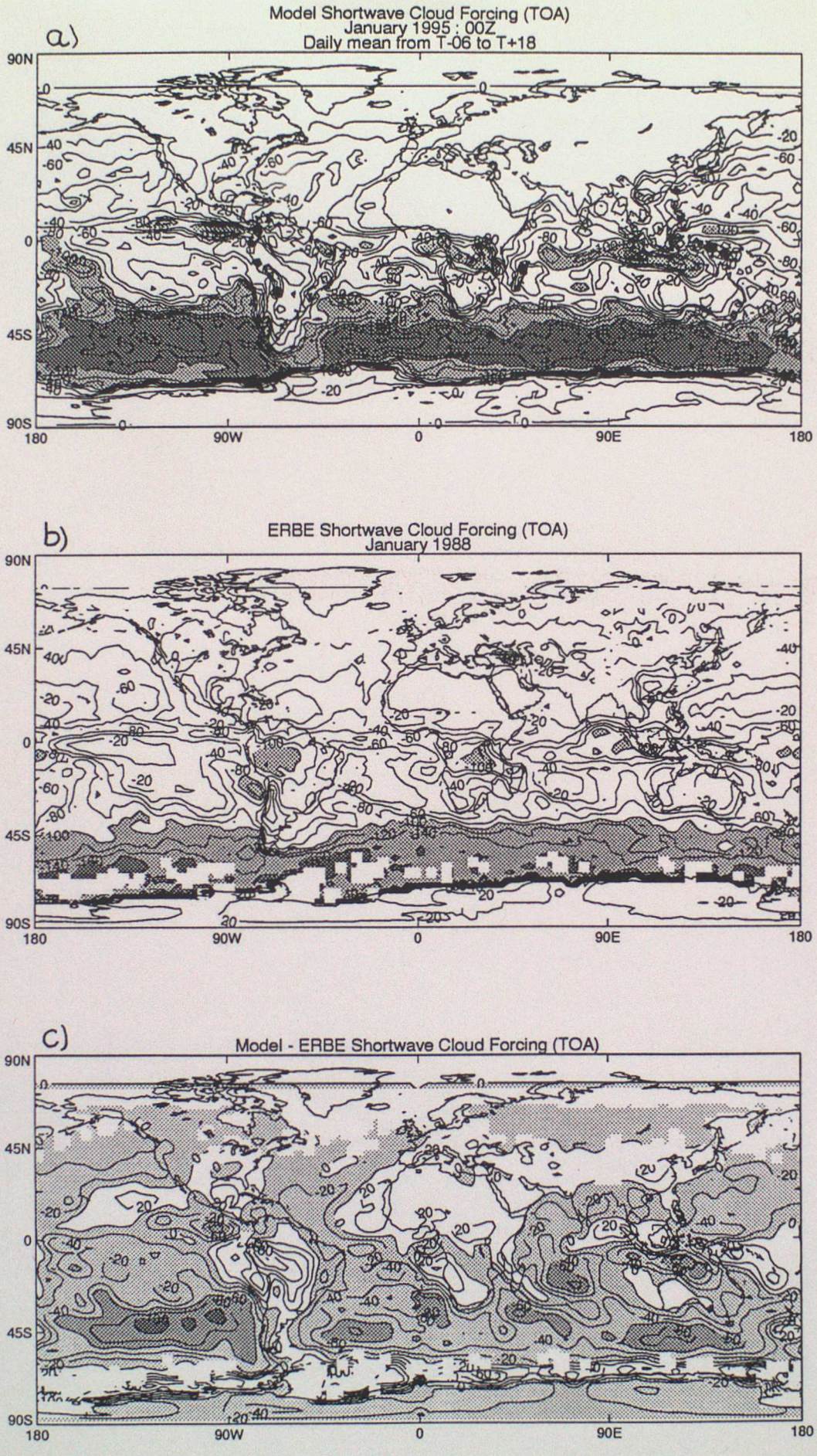
a)
Model Shortwave Cloud Forcing (TOA)
January 1995 : 00Z
Daily mean from T-06 to T+18
b)
ERBE Shortwave Cloud Forcing (TOA)
January 1988
c)
Model - ERBE Shortwave Cloud Forcing (TOA)
90N
45N
0
45S
90S
180
90W
0
90E
180

Figure 17

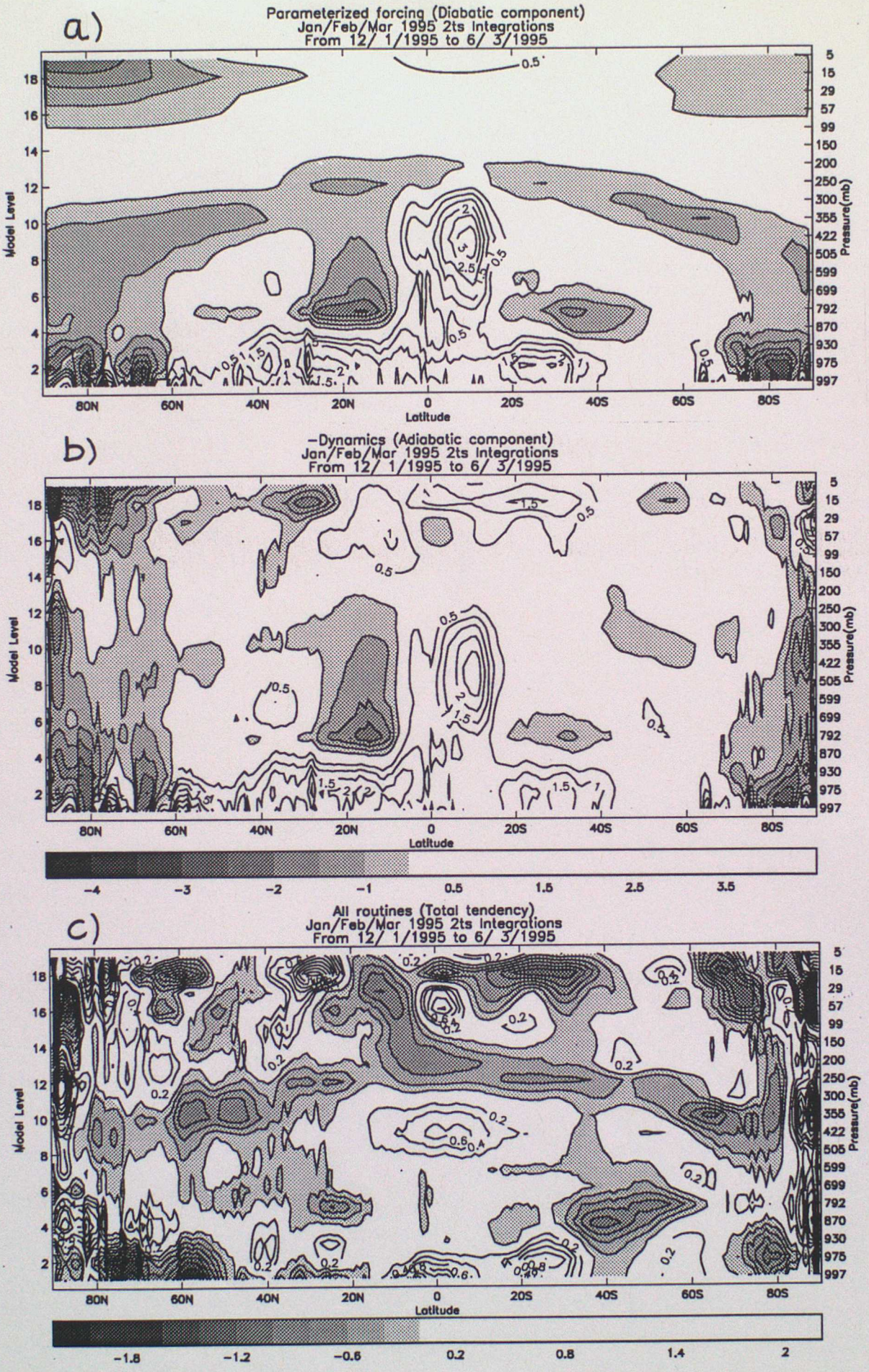
a)
Parameterized forcing (Diabatic component)
Jan/Feb/Mar 1995 2ts Integrations
From 12/ 1/1995 to 6/ 3/1995
b)
-Dynamics (Adiabatic component)
Jan/Feb/Mar 1995 2ts Integrations
From 12/ 1/1995 to 6/ 3/1995
c)
All routines (Total tendency)
Jan/Feb/Mar 1995 2ts Integrations
From 12/ 1/1995 to 6/ 3/1995
Model Level
Pressure(mb)
Latitude
80N
60N
40N
20N
0
20S
40S
60S
80S
5
15
29
57
99
150
200
250
300
355
422
505
599
699
792
870
930
975
997
-4
-3
-2
-1
0.5
1.5
2.5
3.5
-1.8
-1.2
-0.6
0.2
0.8
1.4
2

Figure 18

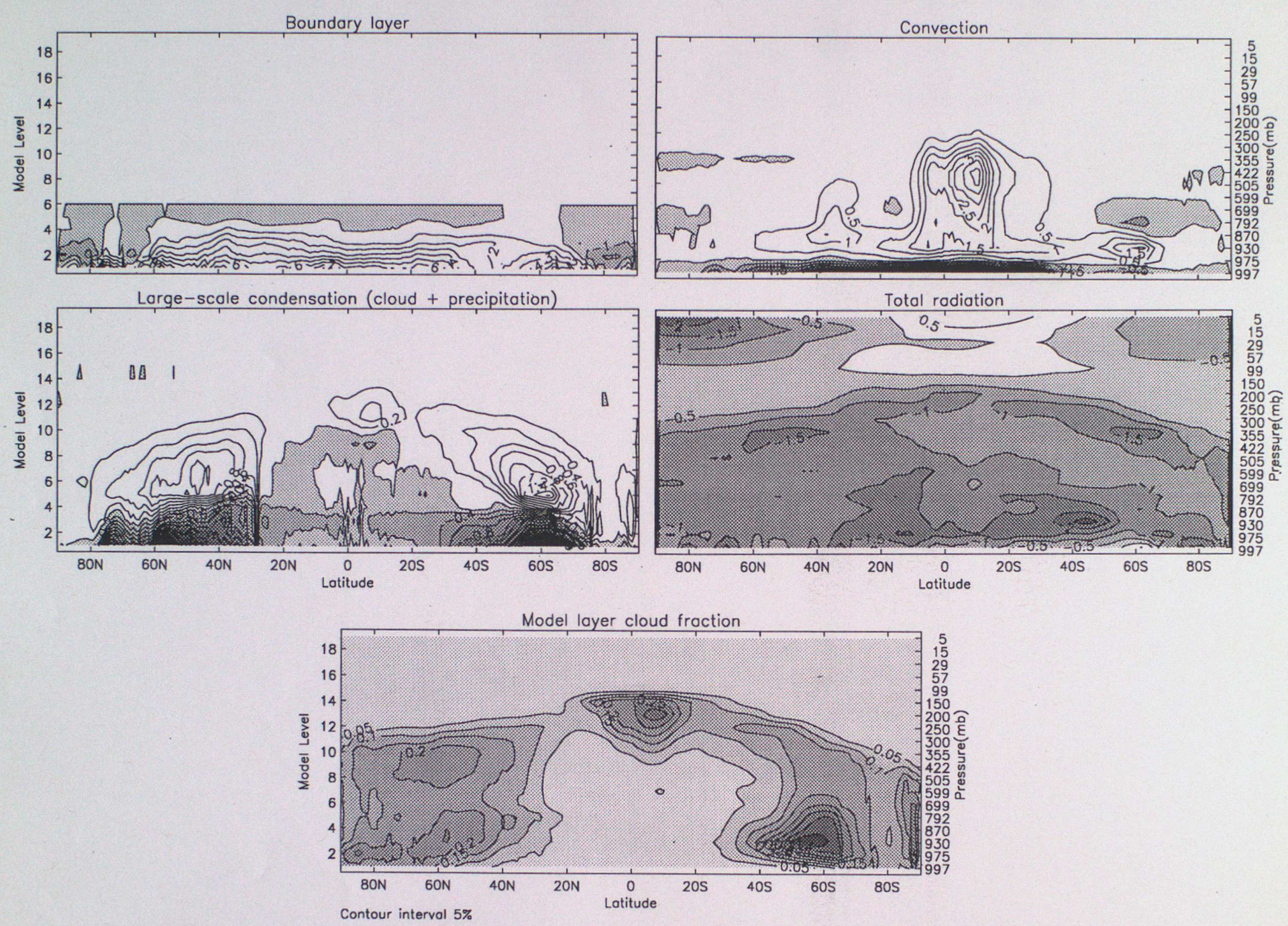
Boundary layer
Convection
Large−scale condensation (cloud + precipitation)
Total radiation
Model layer cloud fraction
Model Level
Pressure(mb)
Latitude
80N
60N
40N
20N
0
20S
40S
60S
80S
Contour interval 5%

Figure 19

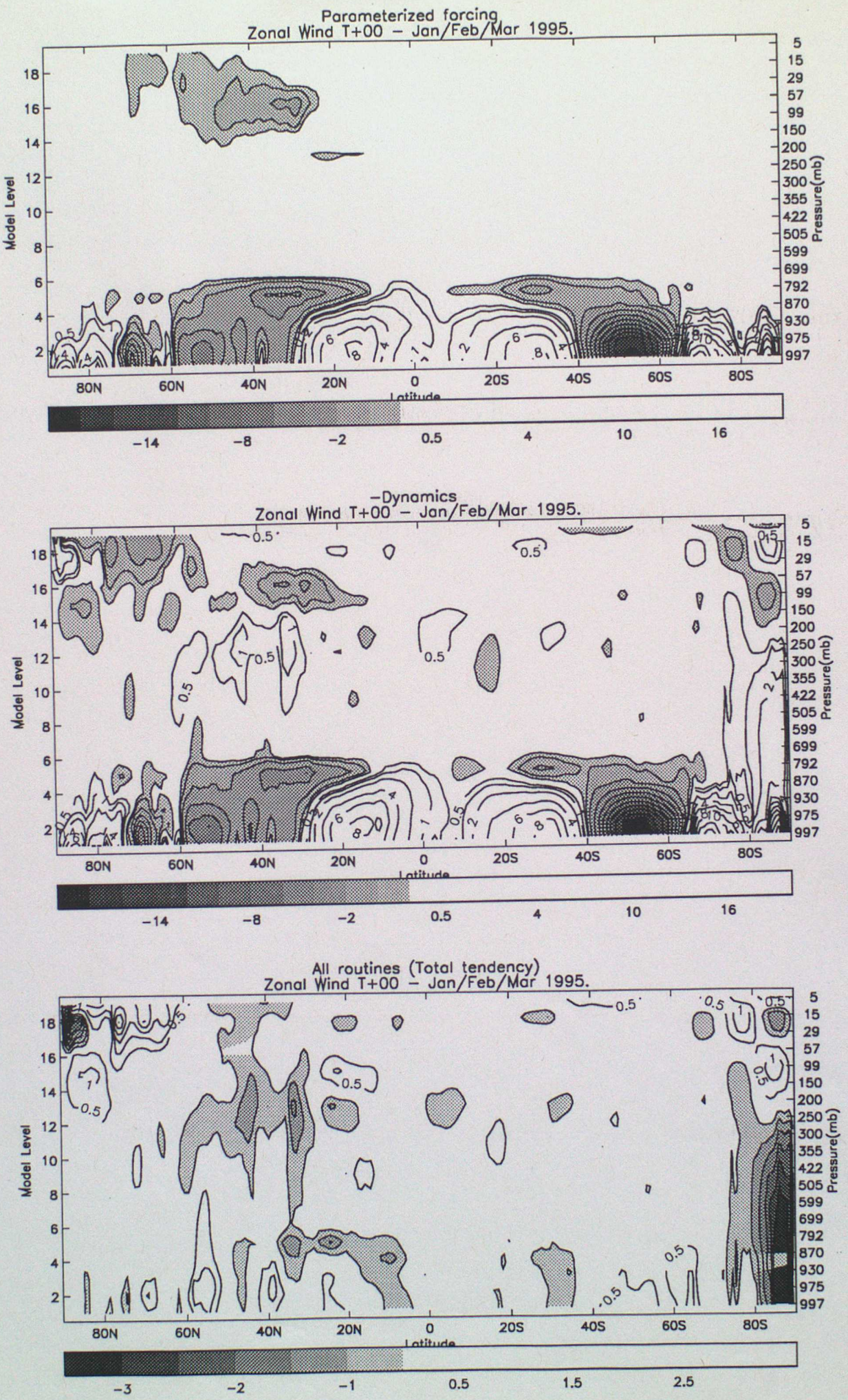
Parameterized forcing
Zonal Wind T+00 – Jan/Feb/Mar 1995.
Model Level
Pressure(mb)
Latitude
80N 60N 40N 20N 0 20S 40S 60S 80S
−14 −8 −2 0.5 4 10 16
−Dynamics
Zonal Wind T+00 – Jan/Feb/Mar 1995.
All routines (Total tendency)
Zonal Wind T+00 – Jan/Feb/Mar 1995.
−3 −2 −1 0.5 1.5 2.5

Figure 20


DJF 94/95
Band Pass S.D. MSLP
T+00
a)
DJF 94/95
Band Pass S.D. MSLP
T+120
b)
Band Pass S.D. MSLP
T+120 – T+00
c)

Figure 21

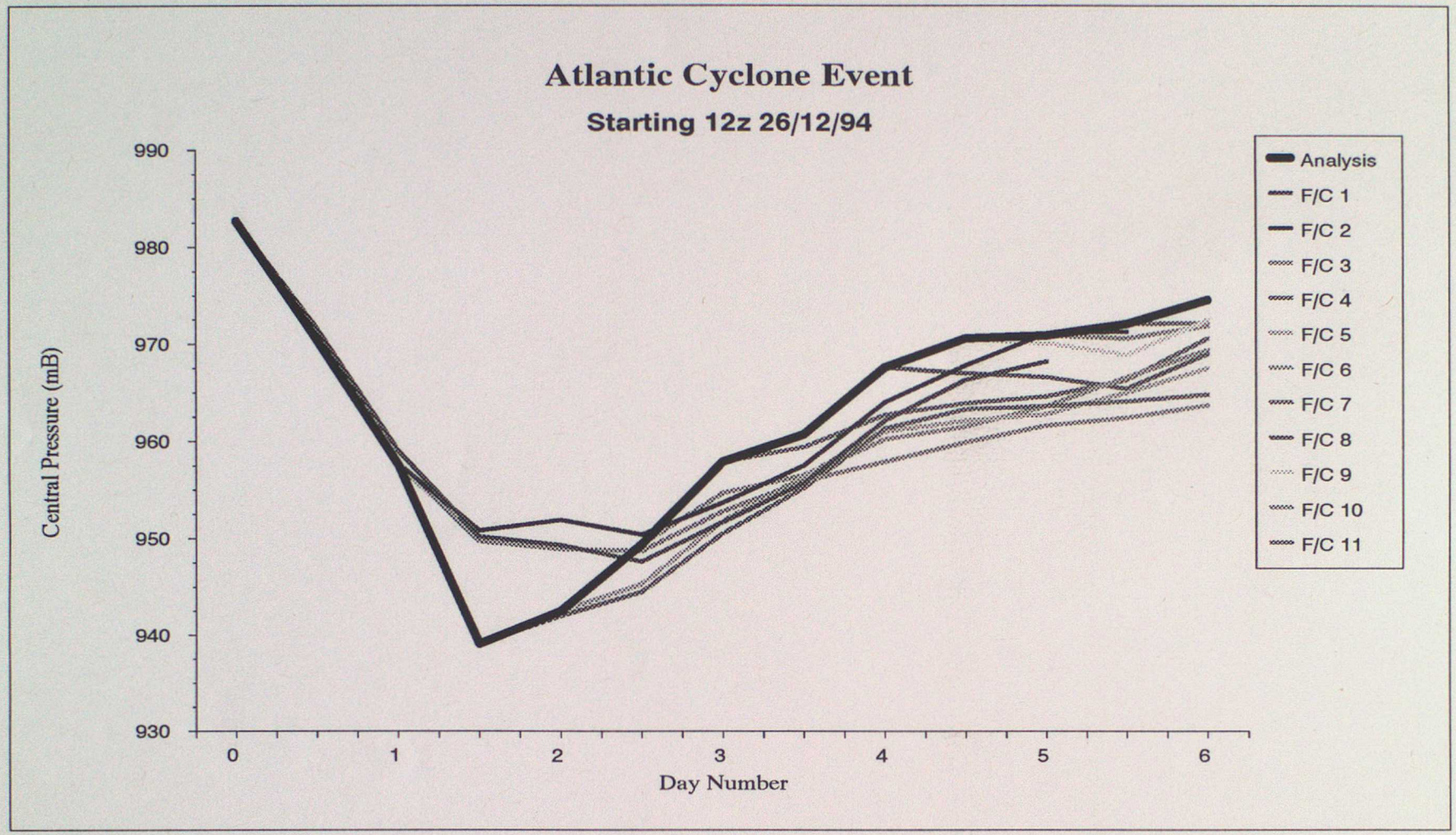
Atlantic Cyclone Event
Starting 12z 26/12/94
Central Pressure (mB)
990
980
970
960
950
940
930
0
1
2
3
4
5
6
Day Number
Analysis
F/C 1
F/C 2
F/C 3
F/C 4
F/C 5
F/C 6
F/C 7
F/C 8
F/C 9
F/C 10
F/C 11

Figure 22

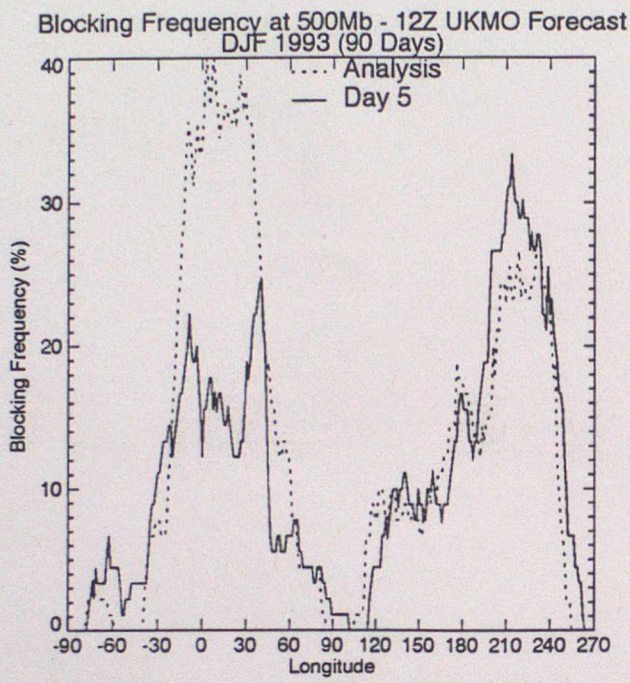
Blocking Frequency at 500Mb - 12Z UKMO Forecast
DJF 1993 (90 Days)
Analysis
Day 5
Blocking Frequency (%)
Longitude

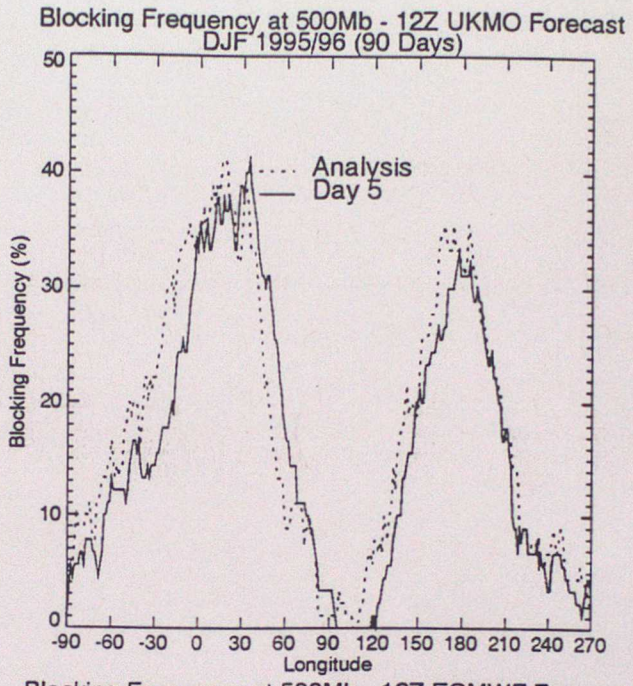
Blocking Frequency at 500Mb - 12Z UKMO Forecast
DJF 1995/96 (90 Days)
Analysis
Day 5
Blocking Frequency (%)
Longitude

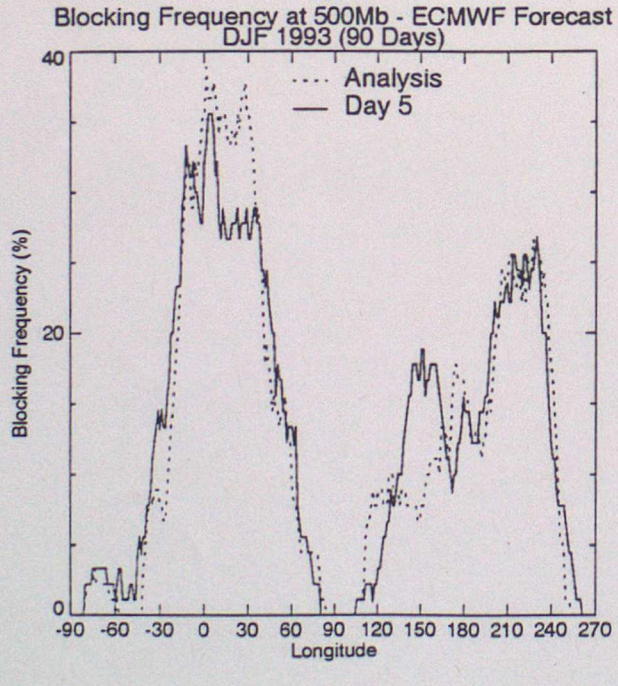
Blocking Frequency at 500Mb - ECMWF Forecast
DJF 1993 (90 Days)
Analysis
Day 5
Blocking Frequency (%)
Longitude

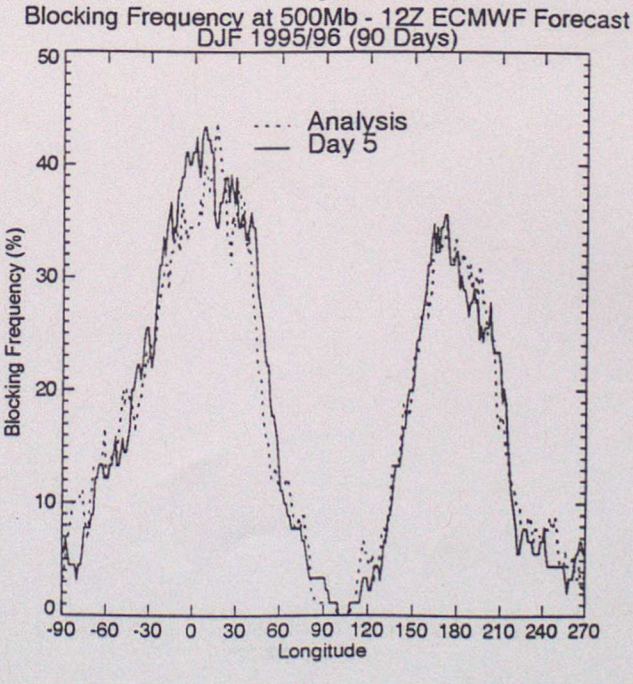
Blocking Frequency at 500Mb - 12Z ECMWF Forecast
DJF 1995/96 (90 Days)
Analysis
Day 5
Blocking Frequency (%)
Longitude

Figure 23

Precipitation Accumulation (mm)
From 1/ 1/1996 to 31/ 1/1996

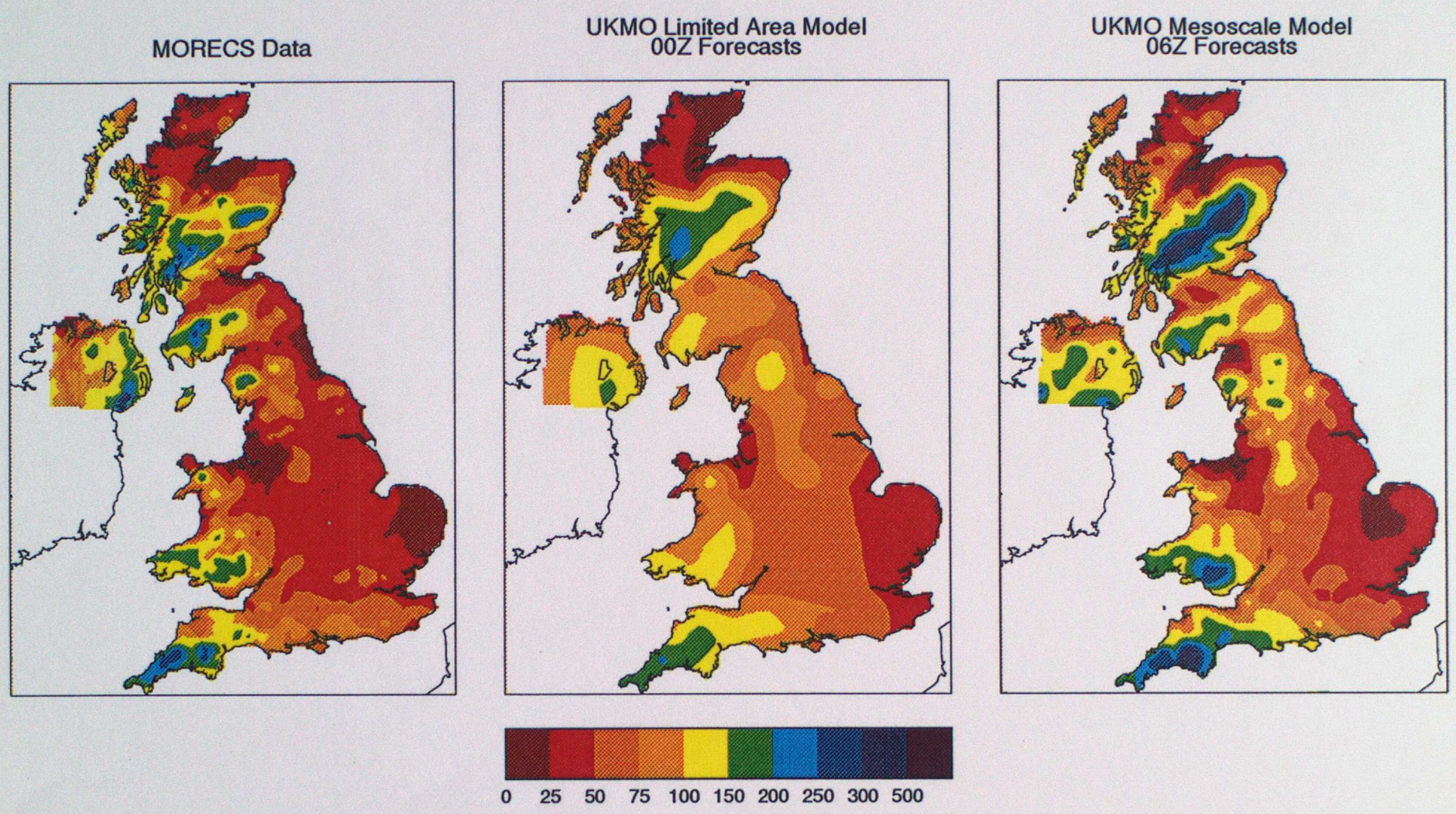

Figure 24

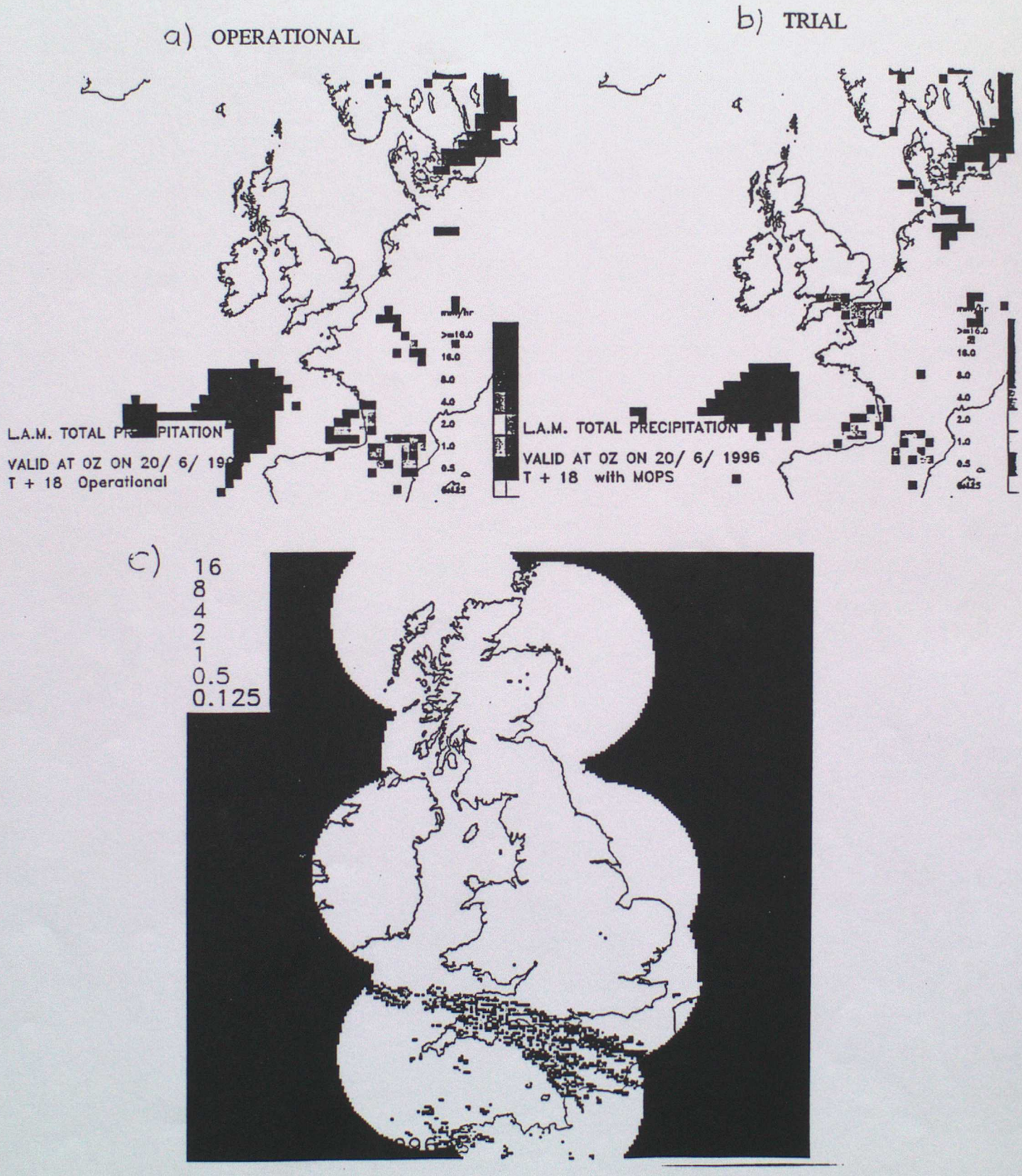
a) OPERATIONAL
b) TRIAL
L.A.M. TOTAL PRECIPITATION
VALID AT 0Z ON 20/ 6/ 1996
T + 18 Operational
L.A.M. TOTAL PRECIPITATION
VALID AT 0Z ON 20/ 6/ 1996
T + 18 with MOPS
c)
16
8
4
2
1
0.5
0.125

Figure 25

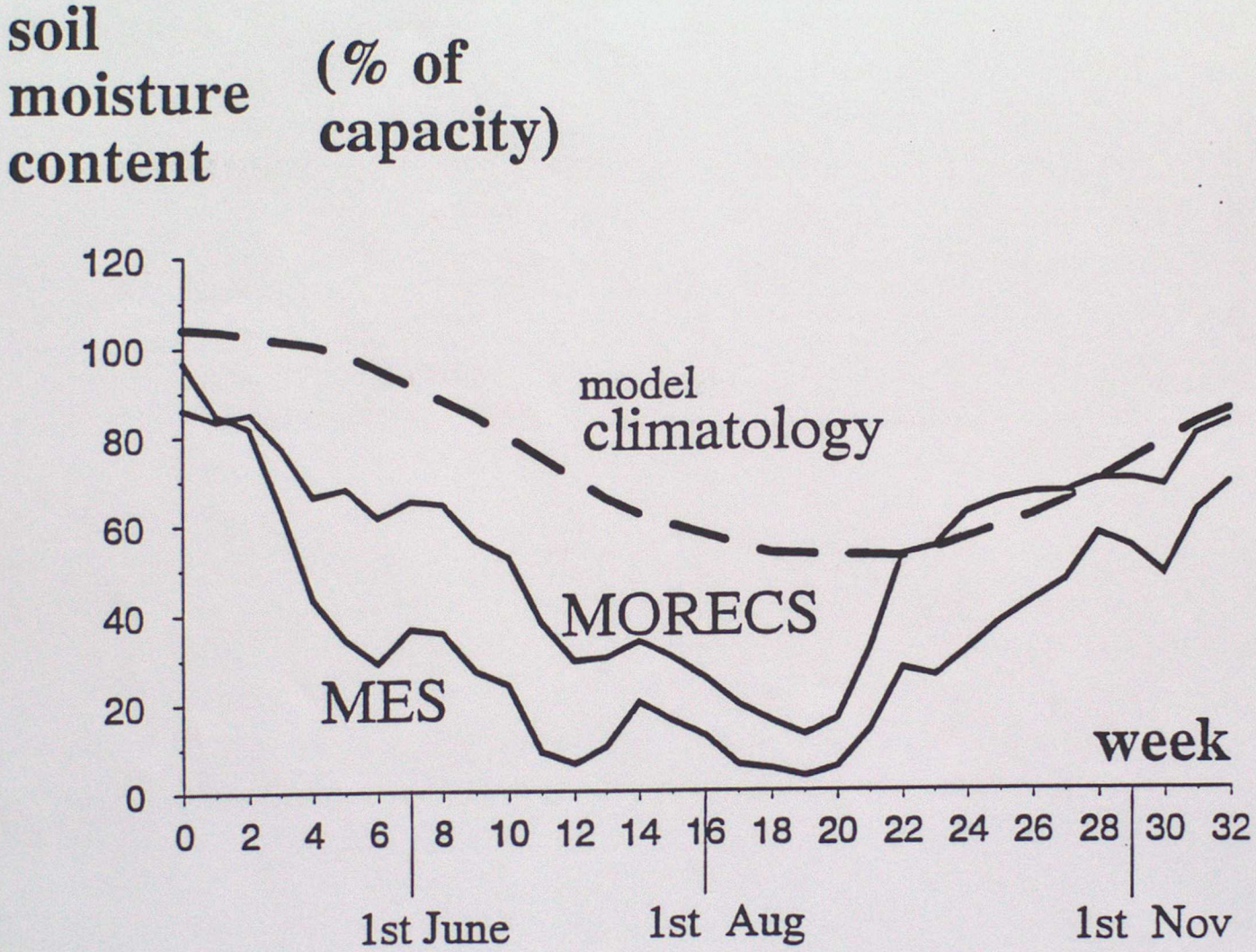
soil moisture content
(% of capacity)
120
100
80
60
40
20
0
model climatology
MORECS
MES
week
0 2 4 6 8 10 12 14 16 18 20 22 24 26 28 30 32
1st June
1st Aug
1st Nov

Figure 26

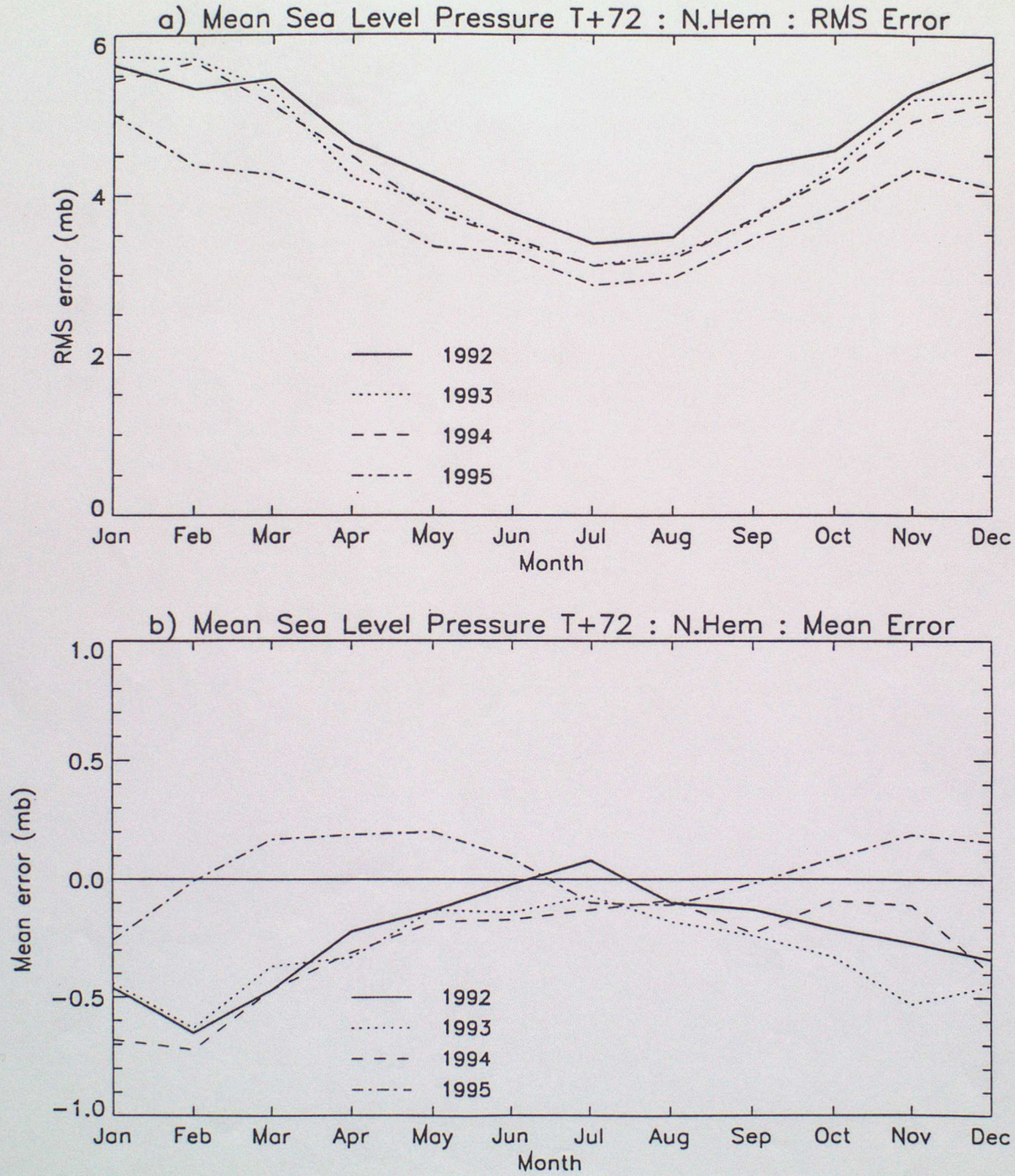
a) Mean Sea Level Pressure T+72 : N.Hem : RMS Error
RMS error (mb)
6
4
2
0
1992
1993
1994
1995
Jan
Feb
Mar
Apr
May
Jun
Jul
Aug
Sep
Oct
Nov
Dec
Month
b) Mean Sea Level Pressure T+72 : N.Hem : Mean Error
Mean error (mb)
1.0
0.5
0.0
−0.5
−1.0
1992
1993
1994
1995
Jan
Feb
Mar
Apr
May
Jun
Jul
Aug
Sep
Oct
Nov
Dec
Month

Figure 27

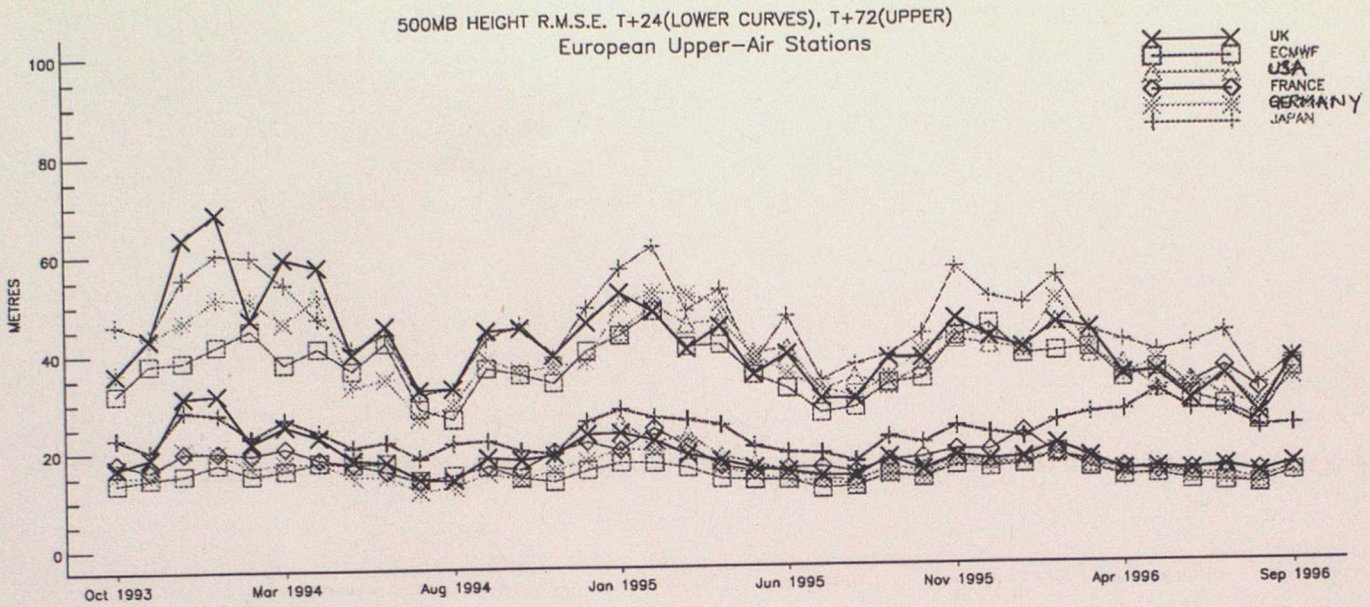
500MB HEIGHT R.M.S.E. T+24(LOWER CURVES), T+72(UPPER)
European Upper–Air Stations
UK
ECMWF
USA
FRANCE
GERMANY
JAPAN
METRES
100
80
60
40
20
0
Oct 1993
Mar 1994
Aug 1994
Jan 1995
Jun 1995
Nov 1995
Apr 1996
Sep 1996

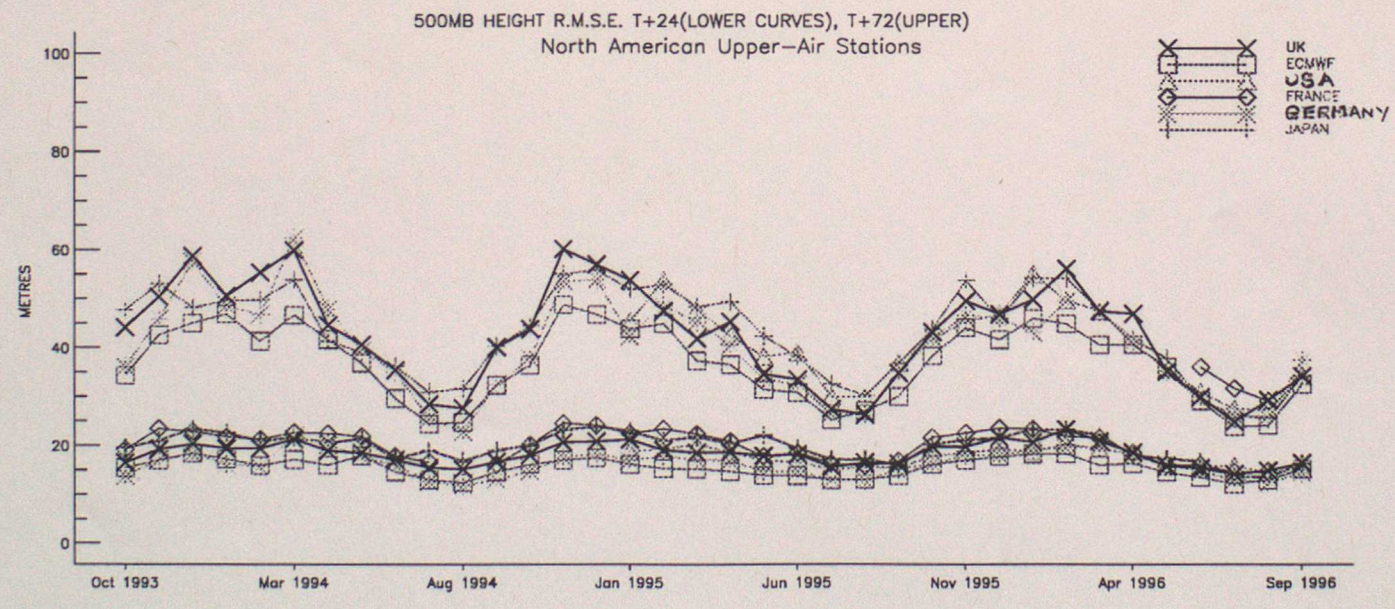
500MB HEIGHT R.M.S.E. T+24(LOWER CURVES), T+72(UPPER)
North American Upper–Air Stations
UK
ECMWF
USA
FRANCE
GERMANY
JAPAN
METRES
100
80
60
40
20
0
Oct 1993
Mar 1994
Aug 1994
Jan 1995
Jun 1995
Nov 1995
Apr 1996
Sep 1996

Figure 28

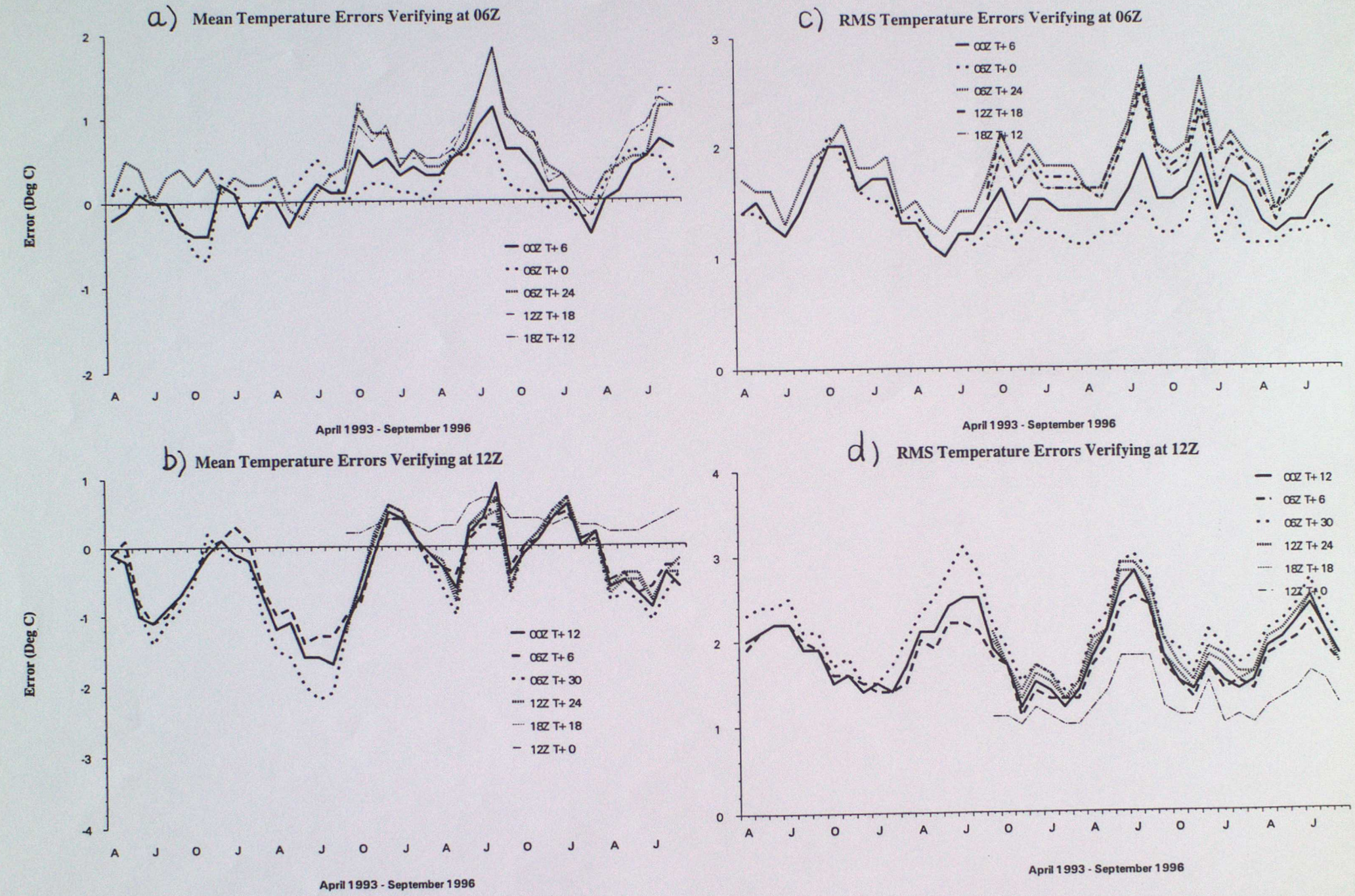
a) Mean Temperature Errors Verifying at 06Z
Error (Deg C)
00Z T+6
06Z T+0
06Z T+24
12Z T+18
18Z T+12
April 1993 - September 1996
b) Mean Temperature Errors Verifying at 12Z
Error (Deg C)
00Z T+12
06Z T+6
06Z T+30
12Z T+24
18Z T+18
12Z T+0
April 1993 - September 1996
c) RMS Temperature Errors Verifying at 06Z
00Z T+6
06Z T+0
06Z T+24
12Z T+18
18Z T+12
April 1993 - September 1996
d) RMS Temperature Errors Verifying at 12Z
00Z T+12
06Z T+6
06Z T+30
12Z T+24
18Z T+18
12Z T+0
April 1993 - September 1996

Figure 29

a) **RMS Vector Wind Errors Verifying at 06Z**

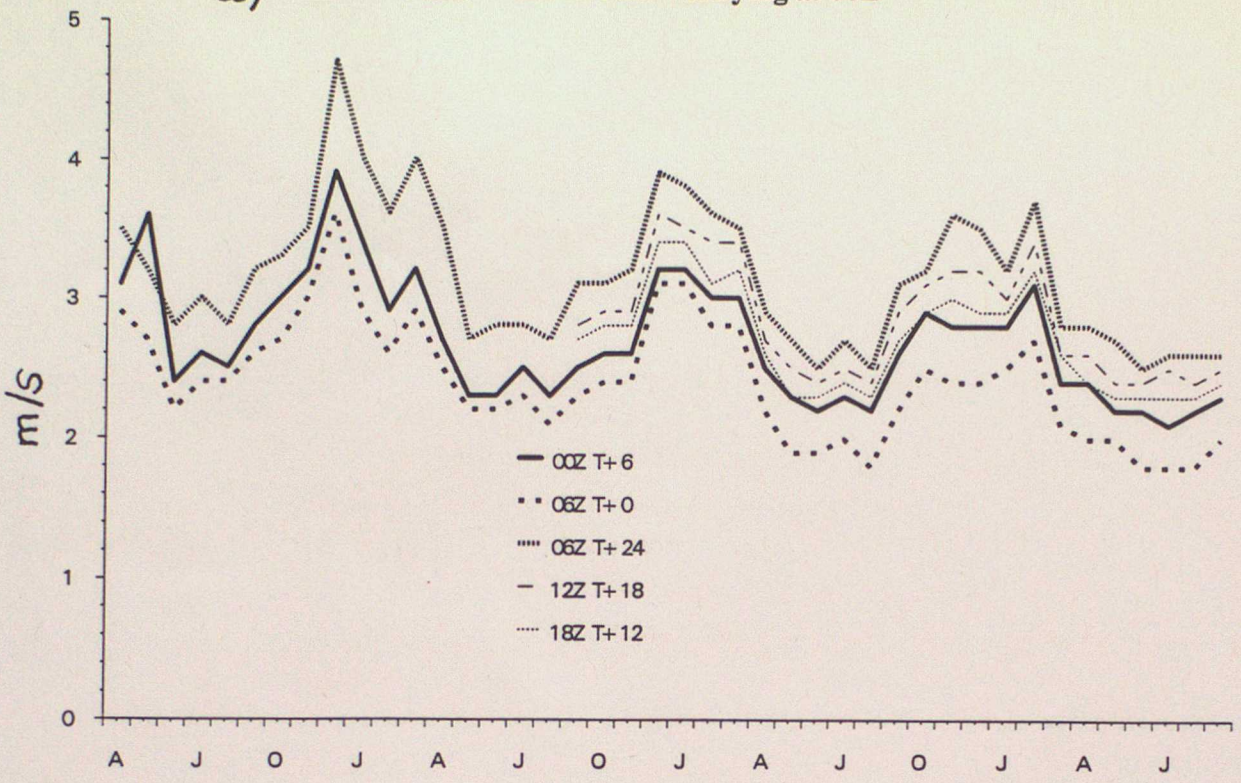

April 1993 to September 1996

b) **Mean Cloud Cover Errors Verifying at 06Z**

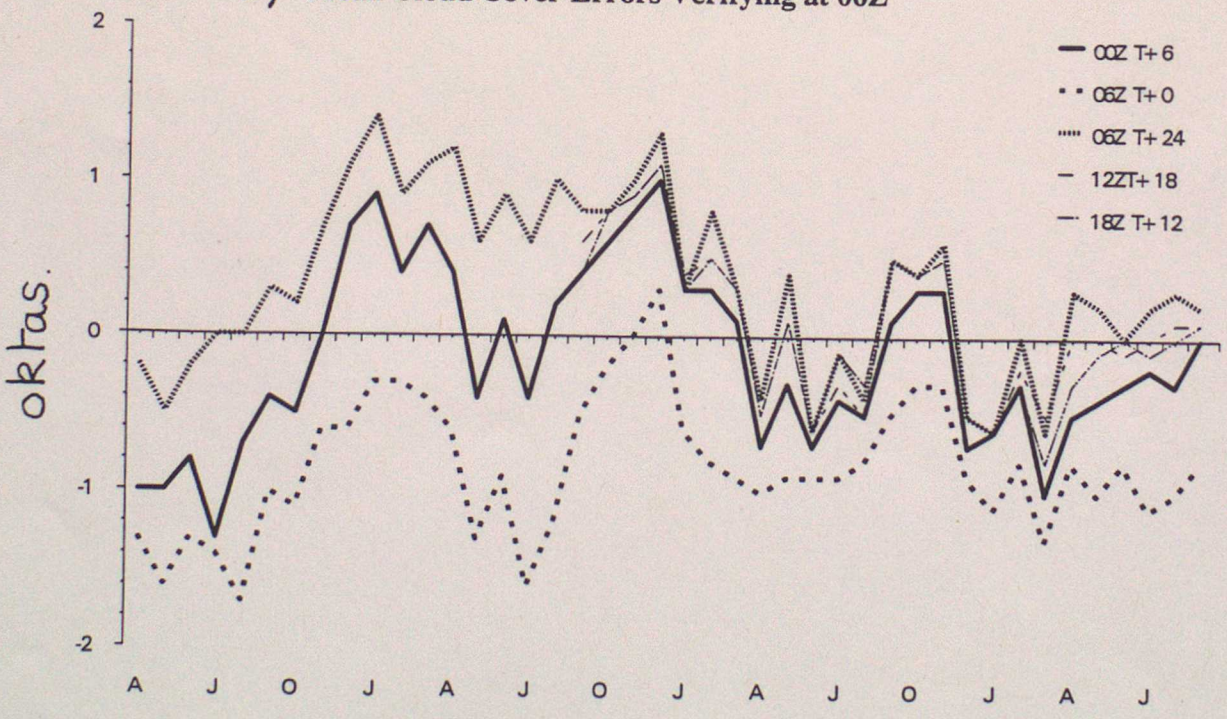

April 1993 - September 1996

Figure 30

Hurricane Bertha

Operational (90km) **60km Resolution**

Analyses valid at 12UTC 12/07/96

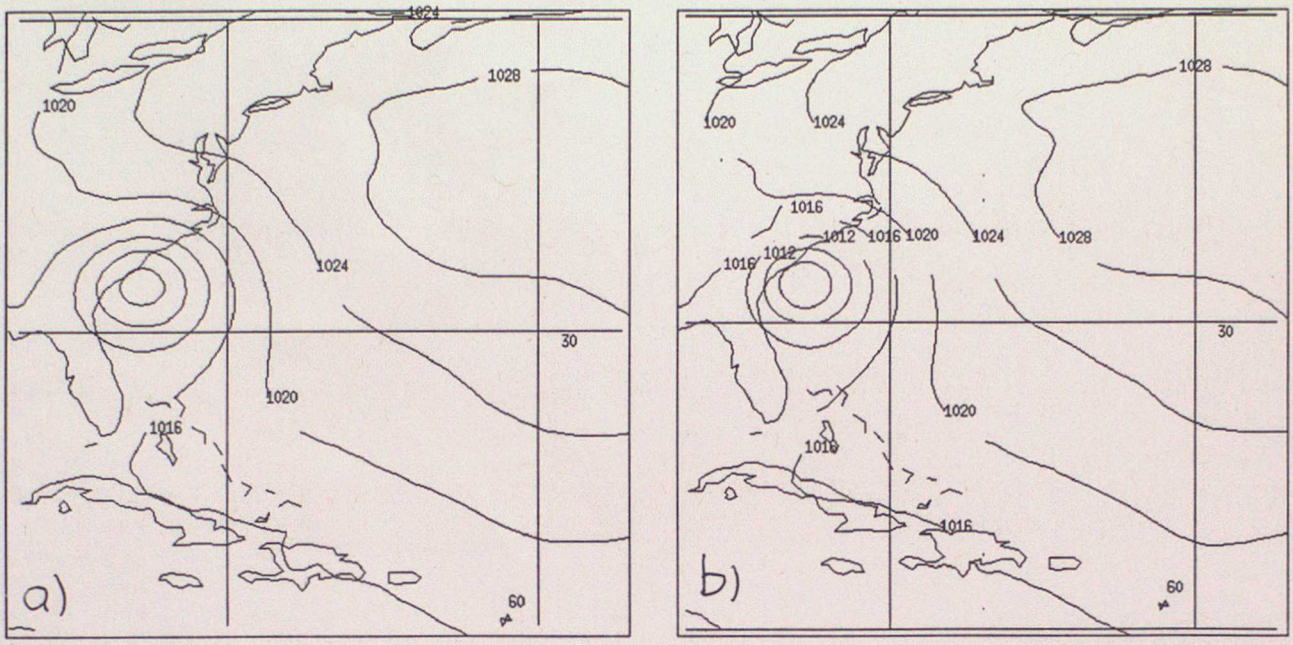

T+72 Forecasts valid at 12UTC 12/07/96

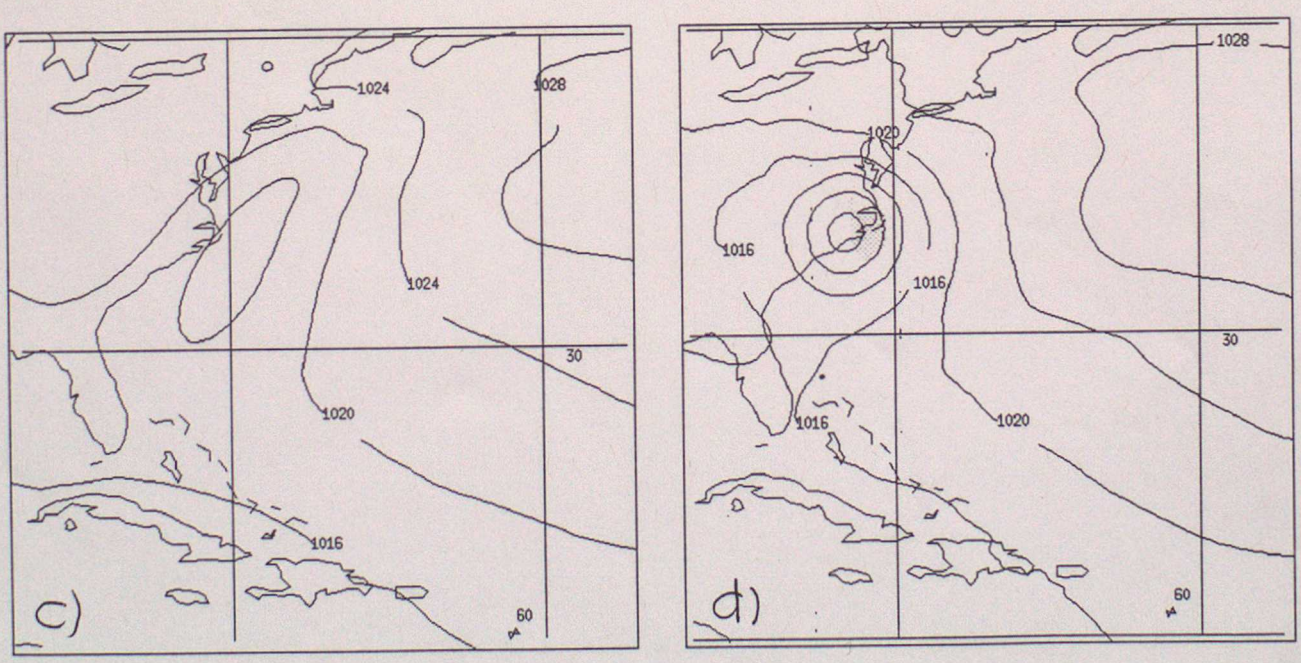

Figure 31